RSC Sustainability

ROYAL SOCIETY OF CHEMISTRY

PAPER

View Article Online
View Journal | View Issue

Cite this: *RSC Sustainability*, 2025, **3**, 2333

Superior proton conductivity and selectivity in sulfonated ionomer biocomposites containing renewably processed and fractionated lignin†

Xueting Wang, [a] Mayura Silva, [b] Colleen Clarke, [a] Bronson Lynn,[a] Mark Robertson,[c] Aidan J. Leopold,[a] Oreoluwa Agede, [a] Lilin He,[d] Stephen Creager, [b] Mark E. Roberts,[a] Mark C. Thies[a] and Eric M. Davis *[a]

Herein, we have synthesized high-performance, low-cost ionomer biocomposites comprised of sulfonated poly(ether ether ketone) (SPEEK) and softwood Kraft lignin. Specifically, SPEEK ionomer composites containing renewably processed and fractionated low and high molecular weight lignin, at concentrations ranging from 5–25 mass%, were synthesized. After fabrication, the water and ion transport properties, as well as the hydrated nanostructure, of the biocomposites were characterized. Most notably, our SPEEK–lignin composite membranes exhibited proton conductivities and proton selectivities that were two-fold and four-fold higher, respectively, than both neat SPEEK and the current benchmark ionomer for these applications, Nafion. In conjunction with ion exchange capacity and equilibrium water uptake data, as well as real-space imaging from electron microscopy, small-angle neutron scattering data suggested that the introduction of lignin increased the spacing between hydrophilic, ionic domains. As a proof of concept, the feasibility of these membranes as proton exchange membranes (PEMs) was assessed. In vanadium redox flow battery (VRFB) tests, SPEEK–lignin membranes containing 15 mass% lignin exhibited performance (power density, discharge voltage) comparable to that of neat SPEEK membranes. This comparable performance underscores the promise of SPEEK–lignin biocomposites as PEMs for next-generation VRFBs.

Received 16th January 2025
Accepted 19th February 2025

DOI: 10.1039/d5su00031a

rsc.li/rscsus

Sustainability spotlight

To advance several UN goals related to affordable, clean, and sustainable energy, a transformative shift in the materials used as ion exchange membranes in energy storage and delivery technologies, such as the redox flow battery, is essential. Addressing the non-renewability and high cost of the current benchmark material – two factors preventing the widescale adoption of this technology – we have fabricated cost-effective ionomers composed of sulfonated poly(ether ether ketone) (SPEEK) and the renewable biopolymer lignin, with lignin concentrations reaching as high as 25 mass%. The raw Kraft lignin used in these membranes was purified and fractionated using renewable ethanol-water solvent mixtures. Despite the high lignin content, our SPEEK–lignin biocomposites demonstrated superior proton conductivity and proton selectivity compared to both neat SPEEK and the current benchmark material, paving the way for entirely biorenewable ionomers.

1 Introduction

With worldwide energy demand on the rise, grid-scale energy storage technologies are needed to facilitate renewable energy – *e.g.*, wind, solar – integration targets without compromising reliable and cost-effective dispatch of energy from the electrical grid.[1] One such technology, the vanadium redox flow battery (VRFB), has garnered significant attention as a scalable energy storage technology as a result of their long cycle life, flexible design, and rapid response time.[2] However, these systems rely on proton exchange membranes (PEMs) that have traditionally been constructed from expensive and non-renewable materials such as Nafion™ ($500–1700/m^{-2} based on the membrane thickness and scale[3–5]). Reducing the cost and environmental footprint of PEMs, while still maintaining this benchmark performance, is paramount to deployment of VRFB technology. Sulfonated poly(ether ether ketone) (SPEEK) has emerged as a promising PEM for VRFBs due to its low cost ($12–80/m^{-2} based on the membrane thickness and scale[6]), as well as

[a]*Department of Chemical and Biomolecular Engineering, Clemson University, Clemson, SC 29631, USA. E-mail: ericd@clemson.edu*

[b]*Department of Chemistry, Clemson University, Clemson, SC 29631, USA*

[c]*School of Polymer Science and Engineering, University of Southern Mississippi, Hattiesburg, MS 39406, USA*

[d]*Neutron Scattering Division, Oak Ridge National Laboratory, Oak Ridge, TN 37830, USA*

† Electronic supplementary information (ESI) available. See DOI: https://doi.org/10.1039/d5su00031a

a comparable proton conductivity with Nafion. When used in redox flow battery stacks, SPEEK membranes have been shown to significantly reduce their overall cost.[5]

While SPEEK is a promising alternative, these ionomers alone still suffer from a high vanadium ion crossover rate, ultimately leading to reduced performance and lifetime for VRFBs constructed with SPEEK PEMs.[6] To combat this issue and make PEMs more renewable, recent investigations have begun exploring the use of the lignin, a renewable and uniquely aromatic biopolymer, as an additive.[7] Lignin is an abundant and naturally occurring source of phenolic compounds and functional groups – *e.g.*, hydroxyl, carboxylic acid – that impart lignin with a variety of attractive properties.[8,9] However, the lignin recovered from pulp mills has a complex, heterogeneous structure, a broad molecular weight (MW) distribution, which typically necessitates the need for further processing to produce a final lignin with acceptable performance properties. As such, previous investigations of SPEEK–lignin PEMs have been unable to elucidate the fundamental structure–property relationships that govern their transport properties due to the use of poorly defined, unfractionated, off-the-shelf lignins.[10–12] In addition, the proton conductivities of the SPEEK–lignin composite membranes produced in these previous studies were relatively low (between 20 and 30 mS cm^{-1}) when compared to the current benchmark ionomer Nafion (between 80 to 100 mS cm^{-1}).

In this work, we leverage the Aqueous Lignin Purification using Hot Agents (ALPHA) process to fractionate a papermill Kraft lignin *via* a unique liquid–liquid equilibrium that forms upon heating. Using a renewable solvent system (ethanol/water) for this fractionation, both a low molecular weight (LMW) fraction, with MW ≈ 5470 g mol^{-1}, and a high molecular weight (HMW) fraction, with MW ≈ 34 500 g mol^{-1} were produced with ALPHA from the feed Kraft lignin (MW ≈ 18 260 g mol^{-1}) to evaluate within SPEEK–lignin PEMs. These well-defined lignin fractions allowed us to complete the most thorough investigation into the effects of SPEEK–lignin interplay on PEM properties to date. Specifically, different mass loadings of either LMW or HMW lignin (5, 15, and 25 mass%) and different charge group densities (*i.e.*, degrees of sulfonation of SPEEK) were able to be related to critical PEM properties such as ion exchange capacity (IEC), equilibrium water uptake (EWU), proton conductivity, and vanadium ion permeability. Additionally, the lignin dispersion state was directly imaged *via* transmission electron microscopy (TEM) and the hydrated phase segregated nanostructure of these hybrid ionomer membranes was characterized using small-angle neutron scattering (SANS). Finally, VRFBs were evaluated using membranes comprising SPEEK or SPEEK–lignin ionomers by measuring the discharge voltage with increasing current density to determine the power output over a range of operating conditions.

2 Experimental

2.1. Materials

Poly(ether ether ketone) (PEEK) was purchased from Victrex (Lancashire, United Kingdom), with the trade name "VICTREX PEEK 450PF". The PEEK had a weight-average molecular weight of 105 000 g mol^{-1} and dispersity of approximately 3. The feed (bulk) lignin used for these experiments was a softwood Kraft lignin obtained from Domtar (South Carolina, USA), with the trade name "BioChoice™". Hydrogen peroxide (30 wt% in H_2O), sulfuric acid (H_2SO_4; 98%, ACS reagent), *N*,*N*-dimethylacetamide (DMAc; for HPLC, ≥99.5%), deuterated dimethyl sulfoxide (DMSO-d6), vanadium(IV) oxide sulfate hydrate (97%), magnesium sulfate (anhydrous), deuterated chloroform, chromium(III) acetylacetonate, 2-chloro-4,4,5,5-tetramethyl-1,3,2-dioxaphospholane (TMDP) and sodium chloride were purchased from Sigma-Aldrich. Molecular biology-grade 200 proof ethanol (Cat. No. BP28184) was obtained from Fisher Scientific. *N*,*N*-dimethylformamide (DMF) and 0.2 μm polytetrafluoroethylene (PTFE) syringe filter were purchased from VWR. *N*-Hydroxy-5-norbornene-2,3-dicarboximide was purchased from TCI America. Lithium bromide (LiBr) was purchased from Alfa Aesar. Pyridine was purchased from Acros Organics. The water used for all experiments and synthesis of the ionomer membranes was reverse osmosis (RO) water (resistivity ≈ 18 MΩ cm).

2.2. Lignin fractionation *via* the aqueous lignin purification using hot agents (ALPHA) process

Prior to fractionation *via* the ALPHA process, the feed lignin was dried at 90 °C until no weight change was observed. The ALPHA step was performed in a 50 mL Parr reactor (Model no. 4843, Moline, IL) using a 50 wt% ethanol:water solution combined with the feed BioChoice™ lignin (BCL) at a solvent : lignin ratio of 3 : 1. The lignin solution was then sealed and mixed in the reactor, and the temperature was increased to 45 °C, where it was held for 30 min to create the two liquid phases that are characteristic of the ALPHA process. After the time elapsed, the lower molecular weight (LMW) solvent-rich phase was decanted off from the higher molecular weight (HMW) lignin-rich liquid phase. These two phases were then dried in the same manner as the feed lignin, after which the lignin was ground into a powder with a mortar and pestle after drying was complete. The weight-average molecular weights of the BCL, LMW lignin, and HMW lignin are 18 200 g mol^{-1}, 5470 g mol^{-1}, and 34 500 g mol^{-1}, respectively.

2.3. SPEEK–lignin composite membrane synthesis

Prior to the sulfonation reaction, approximately 4 g of PEEK powder was dried at room temperature under dynamic vacuum for 24 h. After drying, the PEEK powder was slowly added to 60 mL of H_2SO_4 and the mixture was stirred at room temperature until a clear, homogenous solution was obtained (≈2 h). Next, the temperature of the PEEK–H_2SO_4 solution was increased to 50 °C and held there for either 3 h or 4 h, depending on the desired degree of sulfonation, to obtain SPEEK. Note, the PEEK–H_2SO_4 solution was mixed using a mechanical stirrer at ≈350 rpm. Following sulfonation, the final SPEEK was precipitated by pouring the solution SPEEK–H_2SO_4 into cold (with ice) RO water, after which the precipitate was washed >10× with RO water to remove residual sulfuric

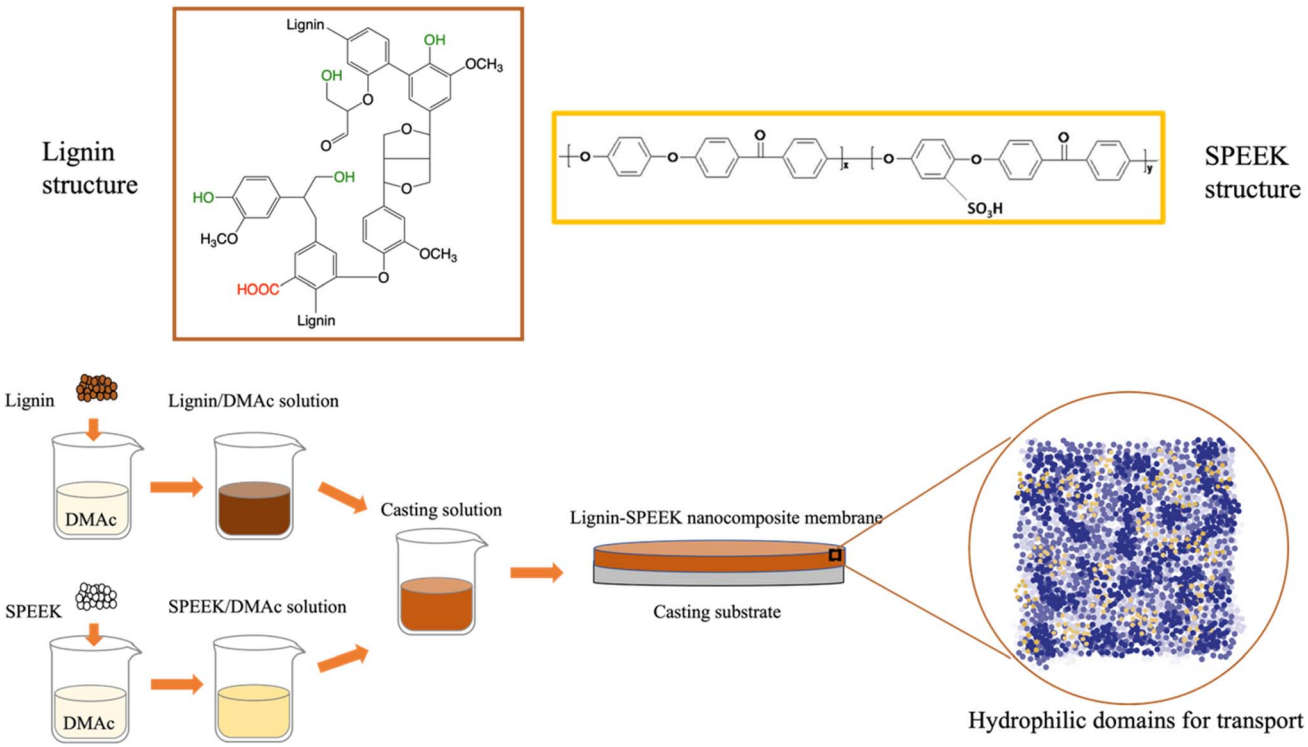

Fig. 1 Illustrative schematic of SPEEK–lignin composite membrane synthesis procedure.

acid. The precipitate was then dried under dynamic vacuum at room temperature for ≈30 hours. Prior to use in membrane fabrication, the fractionated lignin with different molecular weights was dried under dynamic vacuum at room temperature overnight. An illustrative schematic of the synthesis route used to fabricate the SPEEK–lignin composite membranes is shown in Fig. 1.

To prepare the casting solution, a specified amount of dried SPEEK was dissolved in DMAc at a concentration of 10 mass% (here, mass% = $m_{SPEEK}/(m_{SPEEK} + m_{DMAc})$). Next, the SPEEK–DMAc and lignin–DMAc solutions were mixed to obtain the casting solution for a specified lignin concentration in the SPEEK–lignin composite membranes. The obtained solution was sonicated for 2 hours prior to casting to ensure both the lignin and SPEEK were uniformly dispersed in the solution. Next, the SPEEK–lignin–DMAc solution was poured onto a polished quartz substrate that was placed on heating plate set at 80 °C, after which the substrate was covered by a funnel with Kim-wipe flue to allow evaporation of DMAc overnight. Once the solvent was evaporated, the ionomer membranes were annealed at 140 °C under dynamic vacuum for two hours, after which both the vacuum pump and the oven were turned off, and the oven was allowed to cool to room temperature under static vacuum. Prior to experimental measurements, the membranes were equilibrated in RO water for 3 days. The thicknesses of the hydrated SPEEK–lignin membranes were on the order of ≈100 μm. We note that the membranes in each series were fabricated using lignin from the same (single) batch. That is, all the LMW lignin and HMW lignin needed to complete this study were obtained from a single fractionation.

2.4. Nuclear magnetic resonance (NMR) analysis of fractionated lignin

Nuclear magnetic resonance (NMR) spectra were performed on a Bruker NEO 500 MHz spectrometer equipped with a Bruker SmartProbe for ^{1}H (500 MHz, DMSO-d_6) and ^{31}P (500 MHz, $CDCl_3$). ^{1}H NMR was used to obtain the degree of sulfonation (DS) of the SPEEK, while ^{31}P NMR was used to obtain the functional group content for each lignin fraction. For ^{1}H NMR, ∼3 mass% polymer solution was prepared in deuterated dimethyl sulfoxide (DMSO-d_6). For ^{31}P NMR, the integration regions of interest, as well as the specific ^{31}P NMR procedure, have been previously described.[13–16]

2.5. Characterization of the lignin molecular weight

The weight-average molecular weights of the BioChoice™ lignin (BCL), as well as the two lignin fractions obtained from the ALPHA process (*i.e.*, low molecular weight (LMW) lignin and high molecular weight (HMW) lignin) were determined by gel permeation chromatography (GPC) (Agilent 1200 series) with a DAWN MALS (Multi-Angle Light Scattering) detector (Dawn Heleos II Ambient with COMET, WH-2 C, Wyatt Technologies), utilizing a 785 nm laser and bandwith filters, for absolute weight-average molecular weight determination. First, approximately 7.5 mg of each lignin fraction, air-dried in a fume hood and finely ground using a mortar and pestle, was added to 5 mL of the mobile phase which consists of 0.05 mol L^{-1} of LiBr in DMF. This solution was sonicated for approximately three hours and 1.5 mL of the solution was filtered through a 0.2 μm polytetrafluoroethylene (PTFE)

syringe filter (VWR 28145-291) into a 2 mL vial with screw top caps with PTFE pre-slit septa (Microsolv, 9502S-WCV). 100 μL of the filtered samples were then injected into the GPC mobile phase at a flowrate of 0.6 mL min^{-1}. Two columns in series were used for separation; a Waters Styragel HT 5 (WAT044214) column, followed by an Agilent PolarGel-L (PL1117-6830) column. The GPC chromatographs of the various lignin fractions and the polystyrene standard, along with data of the 25 000 g mol^{-1} polystyrene standard used to generate the molecular weight calibration curve, are provided in the ESI.†

2.6. Vanadium (vanadyl) ion permeability

The vanadium (vanadyl) ion (VO^{2+}) permeability of each ionomer membrane was characterized as previously described.[17,18] Briefly, the membrane was placed in a diffusion cell (Franz cell from Permegear; Bethlehem, PA), which had donating and receiving reservoirs filled with a solution of 1.5 mol per L $VOSO_4$ in 3 mol per L H_2SO_4 and a solution of 1.5 mol per L $MgSO_4$ in 3 mol per L H_2SO_4, respectively. Aliquots were taken from the receiving reservoir at various time points, and the concentration of VO^{2+} was measured using an ultraviolet-visible (UV-vis) spectrometer (VWR UV-3100PC). UV-vis scans were taken over the wavelength range of 400 nm to 1100 nm. Note, these experiments were carried out at room temperature. The permeability of VO^{2+} was calculated *via* the following equation

$$V_R \frac{dC_R(t)}{dt} = A\frac{P}{L}C_D, \quad (1)$$

where V_R is the volume of receiving cell, P is the permeability of VO^{2+} ions, $C_R(t)$ and C_D are the VO^{2+} ion concentrations in the donating and receiving cells, respectively. Finally, A and L are the area and thickness of the membranes, respectively.

2.7. Proton conductivity

To characterize proton transport in these ionomer composites, the through-plane proton conductivity was measured with a symmetric electrochemical hydrogen pump (H-pump) cell. Note, all membranes were equilibrated in RO water prior to conductivity experiments, and all experiments were carried out at room temperature and a relative humidity of 100%. The experimental data were collected using a Wave-Driver 20 potentiostat/galvanostat system (Pine Research Instrumentation) and analyzed using the data organizer software AfterMath (Pine Research). The proton conductivity of the SPEEK–lignin composites was calculated using the following equation

$$\kappa = \frac{d}{RA}, \quad (2)$$

where κ, d, and R are the conductivity, thickness, and resistance of the composite, respectively, and A is the geometric active area of the electrodes. Additional information regarding the procedure and the H-pump cell, along with an illustrative schematic, can be found elsewhere.[19]

2.8. Equilibrium water uptake (EWU)

The EWU (in%) of each ionomer biocomposites was calculated *via* the following equation

$$\text{Equilibrium Water Uptake(EWU)} = \frac{m_{wet} - m_{dry}}{m_{dry}} \times 100\%, \quad (3)$$

where m_{dry} and m_{wet} are the dry and wet masses of the membrane. To obtain m_{wet}, each membrane was equilibrated in RO water for 24 h, after which the membranes were removed, patted dry with a KimWipe, and the mass was taken. To obtain m_{dry}, the annealed membranes were weighted immediately after taking out from the vacuum oven.

2.9. Ion exchange capacity (IEC)

Ion exchange capacity (IEC) experiments were performed according to literature.[17,20] Briefly, the dried membrane was equilibrated in 1 mol per L sodium chloride (NaCl) for 24 h, after which it was removed, and the remaining solution was titrated with 0.01 mol per L sodium hydroxide (NaOH) with the indicator phenolphthalein (1% in a mixture of water : ethanol at a ratio of 1 : 1 (v/v)). The IEC for each ionomer composite (in mmol g^{-1}) was then calculated using the following equation

$$\text{Ion Exchange Capacity(IEC)} = \frac{V_{NaOH}C_{NaOH}}{m_{dry}}, \quad (4)$$

where V_{NaOH} and C_{NaOH} are the volume and concentration of the titrated NaOH solution, respectively.

2.10. Transmission electron microscopy (TEM) imaging

Imaging was performed using a Hitachi 9500 high-resolution TEM, which was operated at 300 kV, an emission current of 8.0 mA, and a filament of 29.1 V, with a two second exposure time. To prepare samples for TEM, the casting solution (SPEEK–lignin in DMAc) was further diluted with DMAc to obtain a polymer mass fraction between 0.05 mass% to 0.1 mass%. This solution was then drop cast onto a 300 mesh copper grid with a lacey carbon support (Electron Microscopy Services, Hatfield, PA) and allowed to dry at room temperature. The coated copper grid was then annealed at 140 °C for 2 h.

2.11. Small-angle neutron scattering (SANS) experiments

SANS experiments on the ionomer biocomposites were performed on the CG-2 instrument (GP-SANS) at Oak Ridge National Laboratory.[21] Note, all membranes were equilibrated in D_2O for at least 48 h and then placed in demountable cells. The incoming neutron wavelength and the sample-to-detector distance were varied to collect a range of q values ($q = 4\pi \sin\theta/\lambda$), where 2θ and λ are the scattering angle and wavelength of the neutrons, respectively. For this investigation, SANS data were collected over a q range of 0.007 $Å^{-1}$ to 0.57 $Å^{-1}$. The raw data was corrected for detector efficiency, instrument background, empty cell, and thickness of the membrane prior to the azimuthal average to one-dimensional intensities. Porous silica was used to convert the intensities to absolute scale.[22]

2.12. All-vanadium redox flow battery (VFRB) construction and electrochemical characterization

Redox flow batteries from ElectroCell were assembled with 10 cm^2 electrodes (Ceramaterials, GFE-1 specialty felt) and each of the SPEEK or SPEEK-lignin membranes. Electrical tests were performed on an Arbin Instruments (MSTAT21044) battery analyzer and a multi-head peristaltic pump (Chonry) was used to circulate the electrolyte through the cells. Vanadium electrolytes (50 mL tanks) were prepared starting with 1.0 M vanadium(IV) sulfate oxide hydrate ($VOSO_4$, BeanTown Chemicals) in 3.0 M sulfuric acid (Fisher Scientific) in each tank. The battery was charged to 1.8 V at 50 mA cm^{-2}, then held at 1.8 V until the current decreased below 10 mA (catholyte converted to V^{5+} and anolyte converted to V^{3+}). The catholyte was exchanged with the $VOSO_4$ (IV) solution and the battery was again charged to convert the catholyte to V^{5+} and the anolyte to V^{2+}. Polarization curves were developed on fully charged batteries by discharging for 30 s with a 30 s rest from low (0.5 mA cm^{-2}) to high (160 mA cm^{-2}) current densities. Charge–discharge tests were performed by charging at 20 mA cm^{-2} to 1.8 V, then discharging to 1.0 V.

3 Results and discussion

A summary of the various membranes, as well as the nomenclature used for said membranes moving forward is shown in Table 1. Note, the thickness of the membranes prepared in this work was around 70 μm, and at least three separately cast membranes were prepared for each experimental characterization.

The values of DS for the prepared SPEEK were determined *via* both ^{1}H NMR[23] and titration[24] methods, noting that the latter is a less accurate method for determining the DS. For these analyses, the values of DS from ^{1}H NMR for SPEEK with 3 h and 4 h sulfonation reaction time span were 72% and 80%, respectively, while these same values were determined to be 53.8% and 58.7% from titration. Again, these lower values can be attributed to the fact that titration is not a direct measurement of the amount of sulfonic acid groups in the membrane, but instead, provides the number of available (accessible) sulfonic acid group sites for ion exchange. Note, the ^{1}H NMR spectra of both SPEEK membranes are shown in Fig. S1 in the ESI.†

The vanadium ion (vanadyl ion, VO^{2+}) permeability, proton conductivity, and proton selectivity of both the 3 h SPEEK and 4 h SPEEK series of membranes are shown in Fig. 2a–c and d–f, respectively. Note, the dashed line in each figure represents the value of that respective parameter for neat SPEEK (*i.e.*, SPEEK that contains no lignin). As seen in Fig. 2a, the VO^{2+} ion permeability decreased significantly with the introduction of lignin, at all lignin loadings. Most notably, the VO^{2+} ion permeability was observed to decrease approximately six-fold for 15LWM-SPEEK(72%) ($(2.6 \pm 0.3) \times 10^{-9}$ cm^2 s^{-1}), 15HMW-SPEEK(72%) ($(2.7 \pm 0.3) \times 10^{-9}$ cm^2 s^{-1}), and 25HMW-SPEEK(72%) ($(2.6 \pm 0.1) \times 10^{-9}$ cm^2 s^{-1}), when compared to SPEEK(72%) ($(14.8 \pm 1.6) \times 10^{-9}$ cm^2 s^{-1}), indicating that the presence of the fractioned lignin acts to limit the crossover of vanadium ions. For comparison, the VO^{2+} permeabilities of Nafion 117 (extruded membrane) and solution-cast Nafion membranes are $(44.1 \pm 2.8) \times 10^{-9}$ cm^2 s^{-1} and $(8.1 \pm 0.5) \times 10^{-9}$ cm^2 s^{-1}, as reported in literature.[17,25] That is, the above membranes exhibit over an order of magnitude and approximate two-fold reduction when compared to Nafion 117 and solution-cast Nafion, respectively.

Interestingly, from Fig. 2b, SPEEK(72%) membranes containing 5 mass% LMW and HMW lignin exhibited proton conductivities that were approximately 90% and 110% greater than solution-cast, neat SPEEK (dashed line) and Nafion (95.9 ± 6.5 mS cm^{-1}), respectively.[17] Even at a lignin fraction as high as 15 mass%, SPEEK–lignin membranes containing LMW lignin exhibited conductivities that were analogous to both neat SPEEK and Nafion. Further, at the highest lignin loading of 25 mass%, the ionomer composites still exhibited proton conductivities that were >60 mS cm^{-1}. Note, this observed decrease in proton conductivity is more than likely due to an overall decrease in the concentration of charged groups in the

Table 1 Nomenclature for SPEEK and SPEEK nanocomposites containing fractionated and cleaned lignin with different molecular weight and at different lignin contents

Duration of sulfonation reaction [h]	Degree of sulfonation of SPEEK [%]	Lignin fraction [—]	Lignin loading [g lignin/(g SPEEK + g lignin)]	Nomenclature for ionomer biocomposites [—]
3	72	N/A	0 mass%	SPEEK(72%)
		Low molecular weight	5 mass%	5LMW-SPEEK(72%)
			15 mass%	15LMW-SPEEK(72%)
			25 mass%	25LMW-SPEEK(72%)
		High molecular weight	5 mass%	5HMW-SPEEK(72%)
			15 mass%	15HMW-SPEEK(72%)
			25 mass%	25HMW-SPEEK(72%)
4	80	N/A	0 mass%	SPEEK(80%)
		Low molecular weight	5 mass%	5LMW-SPEEK(80%)
			15 mass%	15LMW-SPEEK(80%)
			25 mass%	25LMW-SPEEK(80%)
		High molecular weight	5 mass%	5HMW-SPEEK(80%)
			15 mass%	15HMW-SPEEK(80%)
			25 mass%	25HMW-SPEEK(80%)

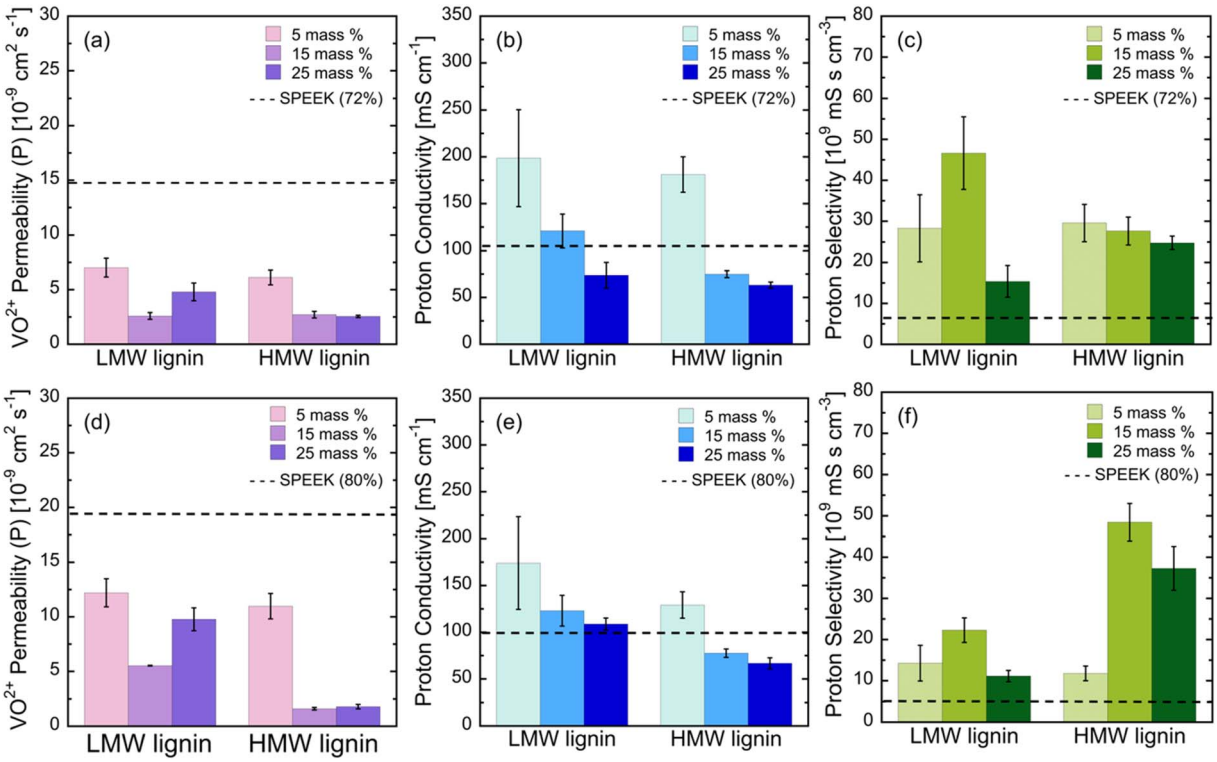

Fig. 2 (a) Vanadyl ion (VO^{2+}) permeability, (b) proton conductivity, and (c) proton selectivity for SPEEK(72%)–lignin nanocomposite membranes. (d) VO^{2+} permeability, (e) proton conductivity, and (f) proton selectivity for SPEEK(80%)–lignin nanocomposite membranes. The dashed lines in each figure represent the average value of that property for neat SPEEK membranes. Note, the error bars represent the standard deviation of the average, which was calculated based on measurements on at least three independent membranes.

ionomer nanocomposite when 25% of the SPEEK (by mass) is replaced by lignin. Finally, one of the most important parameters of merit for PEMs in VRFBs is the proton selectivity, which is defined as the ratio of the proton conductivity to the VO^{2+} permeability. The results of this calculation for the SPEEK(72%) series are shown in Fig. 2c.

As seen from this figure, all lignin-containing ionomers demonstrated higher proton selectivities when compared with the neat SPEEK membrane. Notably, 15LMW-SPEEK(72%) and 15HMW-SPEEK(80%) exhibited proton selectivities that were approximately seven- and 10-fold higher than the corresponding neat SPEEK membranes. Further, when compared to solution-cast Nafion ($(11.9 \pm 1.54) \times 10^{-9}$ mS s cm^{-3}), we observed that all the lignin-containing SPEEK(72%) exhibited improved proton selectivity. When looking at these same data for the lignin-containing SPEEK(80%) (Fig. 2d–f), we observed a similar trend as the SPEEK(72%) series – that is, we observed a reduction in VO^{2+} permeability, higher proton conductivities for membranes containing 5 mass% LMW and HWM lignin, and improved proton selectivities for all lignin-containing ionomer nanocomposites. In addition to the improved proton selectivity of 15HMW-SPEEK(80%), 25HWM-SPEEK(80%) exhibited a proton selectivity that was approximately seven-fold higher than SPEEK(80%) membranes, which again, was also a superior proton selectivity to that of the current benchmark ionomer, Nafion.

Additionally, ion transport in these lignin-containing ionomers was seen to be directly affected by the content of sulfonic acid groups – *i.e.*, the degree of sulfonation. In general, the SPEEK(72%), as well as its lignin-containing counterparts, demonstrated lower VO^{2+} permeabilities when compared to the SPEEK(80%) and its lignin-containing nanocomposites, while surprisingly, higher proton conductivity was observed for SPEEK(72%) based membranes, when compared with their SPEEK(80%) counterpart. We believe that this is directly related to the nanostructure of the membrane, and thus, access to sulfonic acid groups. Results from previous spectroscopic studies[26,27] suggested that VO^{2+} diffusion through these sulfonic acid-based ionomers depends more on the availability of sulfonic acid groups, while the accessibility of sulfonic acid groups is not as critical for proton transport. This also provides some rationale as to why SPEEK(80%) has a higher vanadium ion permeability when compared to SPEEK(72%), though the proton conductivities for SPEEK(72%) and SPEEK(80%) are similar. In addition, investigation of the proton conductivity of SPEEK with varying degrees of sulfonation showed that the conductivity of SPEEK increased when the DS increased from 37% to 72%. However, above a DS of approximately 72%, the proton conductivity was seen to decrease.[28] Similar behavior of decreased proton conductivity at high values of DS has also been observed by other researchers.[23] Further, it must also be noted that post-sulfonation of PEEK results in random, and

Table 2 Functional group content of LMW lignin and HMW lignin fractions as determined from ^{31}P NMR

	Hydroxyl content [mmol OH per g of lignin]						
Lignin type	Aliphatic hydroxyl	Syringyl hydroxyl	Guaiacyl hydroxyl	Hydroxyl-phenyl	Carboxylic acid	Condensed phenolic	Total
LMW lignin	2.12	0.72	2.23	0.32	0.59	4.19	6.89
HMW lignin	2.18	0.79	2.20	0.32	0.45	4.11	6.74

potentially heterogeneous, placement of sulfonic acid groups along the backbone of the polymer.[29] That is, the conductivity of the SPEEK may vary, even at the same value of DS due to the heterogeneity of the fabrication process.

Regarding the impact of lignin MW on ion transport in these membranes, the HMW lignin-containing membranes exhibited lower proton conductivities and lower VO^{2+} permeability for both SPEEK(72%) and SPEEK(80%) series when compared to their LMW lignin-containing counterparts. To provide potential insight into this ion transport behavior, a phosphorylation technique, paired with phosphorus nuclear magnetic resonance (^{31}P NMR) spectroscopy, was employed to quantity the concentration of functional groups (in this case, the hydroxyl and carboxylic acid groups) in each lignin fraction. The ^{31}P NMR spectra of the LMW and HMW lignin are shown in Fig. S2 in the ESI,† while the numerical values obtained from this characterization are listed in Table 2.

As seen from Table 2, the overall hydroxyl group contents of the LMW and HMW lignin fractions are similar, while the carboxylic content of the LMW lignin is approximately 30% higher than that of the HMW lignin. As carboxylic acid groups have been previously leveraged to improve proton conductivity of polymers,[30–33] the higher content in the LMW lignin may help, in part, to explain the improved proton conductivities when compared to their HMW lignin-containing counterparts.

In addition to vanadyl ion permeability and proton conductivity, the equilibrium water uptake (EWU) and the ion exchange capacity (IEC) of each membrane were measured, and the results are presented in Fig. 3. IEC and EWU are important parameters for proton exchange membranes and are both closely tied to ion transport. Conductivity is a measure of the transport of ions (in this case, protons) through the membrane, which has traditionally been thought to occur through two mechanisms: (1) a vehicular mechanism and (2) a Grotthuss

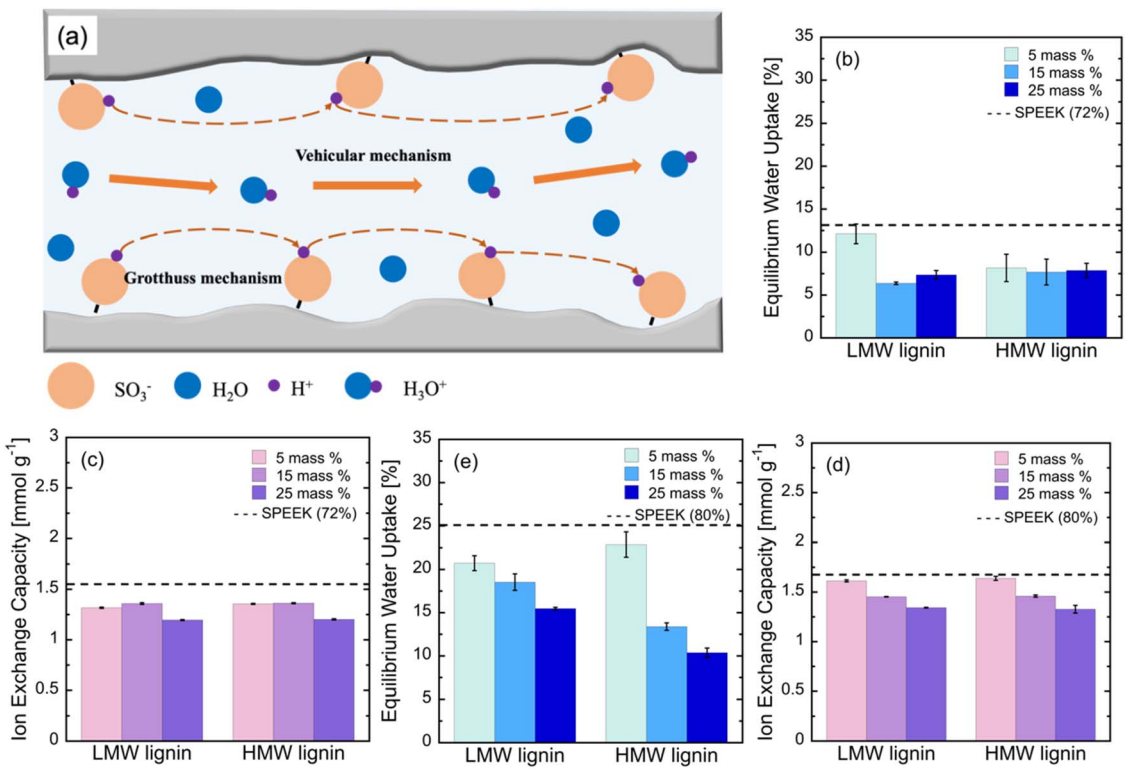

Fig. 3 (a) Proton transport mechanism in hydrophilic channels (b) equilibrium water uptake, and (c) ion exchange capacity for SPEEK(72%) based nanocomposite membranes; (d) equilibrium water uptake, and (e) ion exchange capacity for SPEEK(80%) based nanocomposite membranes. The dashed lines represent the average equilibrium water uptake and ion exchange capacity of neat SPEEK samples. Note, the error bars represent the standard deviation of the average, which was calculated based on measurements on at least three independent membranes.

mechanism (*i.e.*, proton hopping), as illustrated in Fig. 3a. That is, protons move through the hydrophilic domains either by transporting with (*i.e.*, attached to) water molecules, in the hydronium form (H_3O^+), or by hopping between sulfonic acid group sites, where only the interconnected hydrophilic channels allow for proton transport across the membrane, while the sulfonic acid groups isolated within aromatic hydrophobic cages (so-called "dead ends") are unavailable for through-membrane transport.

Along these lines, the IEC of the membrane is a measure of the amount of sulfonic acid groups that are potentially available for proton hopping, and thus is related to the Grotthuss mechanism. Hence, for the same material – *e.g.*, SPEEK, Nafion – a higher IEC typically results in a higher proton conductivity. Furthermore, the EWU can also provide some insight into the proton conductivities as it is a measure of the total amount of water absorbed by the membrane, and in theory, a higher value of EWU would result in higher proton conductivity since vehicular proton transport is a water-facilitated process. Specifically, Fig. 3b–e show the EWU and IEC values for the SPEEK(72%)-based and SPEEK(80%)-based composites, respectively. Again, the dashed line in each figure represents the average of that specific property for neat SPEEK. As seen from these figures, the IEC measured from titration for SPEEK(72%) and SPEEK(80%) are 1.57 mmol g^{-1} and 1.69 mmol g^{-1}, respectively. Interestingly, by using the equivalent weight (EW) of all samples (determined from the DS value obtained from ^{1}H NMR, which provides an accurate measurement of the total amount of sulfonic acid groups present and is not impacted by how these groups phase segregate under hydration), we can obtain an estimate of the amount of inaccessible sulfonic acid groups in the SPEEK membranes.[34] Note that the EW represents the mass of polymers per mole of sulfonic acid groups, where the EW of SPEEK(72%) and SPEEK(80%) were 479 (g SPEEK/mole SO_3H) and 440 (g SPEEK/mole SO_3H), respectively. If we assume that all SO_3H groups in the ionomer are available for proton hopping, the theoretical IEC for SPEEK(72%) and SPEEK(80%) are 2.09 mmol g^{-1} and 2.27 mmol g^{-1}, indicating that approximately 25% of the ion exchange sites are inaccessible in both membranes.

Additionally, the IEC values of all lignin-containing nanocomposites were found to be lower than that of their neat SPEEK counterparts. This is likely related to the decreased amount of accessible charged groups in the membrane. The amount of charged groups (*i.e.*, ionizable functional groups) in these membranes is dependent on the charged group density of each component, that is, the charge group density of the SPEEK and lignin, as well as the ratio of these two components. As seen in Fig. 3 and Table 2, we can directly measure the IEC of neat SPEEK and the content of charged groups in two lignin fractions. The only ionizable functional groups in lignin are the carboxylic acid groups, where the content of this group in LMW and HMW lignin are 0.59 and 0.45 mmol per gram of lignin, respectively. Both values are lower than the charged group (sulfonic acid groups) content in SPEEK. Moreover, carboxylic acid groups only partially ionize in aqueous solution. Thus, the introduction of lignin decreases the total amount of charged groups in the nanocomposites, leading to decreased ion exchange capacity, which is generally correlated with the lignin content, though this is most obvious in the SPEEK(80%)-based composites (see Fig. 3d). It is worth pointing out that while the IEC values of 5LWM-SPEEK(72%), 5HMW-SPEEK(72%), 5LWM-SPEEK(80%), 15LWM-SPEEK(80%), and 5HWM-SPEEK(80%) were lower than that of their neat SPEEK counterparts, the proton conductivities of all these lignin composites were higher than both neat SPEEK and the current benchmark ionomer, Nafion.

Along with the IEC, the values of EWU for SPEEK(72%) and SPEEK(80%) are presented in Fig. 3b and d, respectively. In general, the introduction of lignin leads to a reduction in EWU for all SPEEK–lignin composites, apart from 5LMW-SPEEK(72%) and 5HMW-SPEEK(80%), which both exhibited similar EWU values to the neat counterparts. In addition, we observed that the EWU values of SPEEK(80%) series were significantly higher than the SPEEK(72%) series, which is consistent with the IEC data (Fig. 3c *vs.* e), where, in general, the SPEEK(80%) series membranes demonstrated higher IECs. These data are somewhat contradictory to the measured proton conductivities of ionomers containing 5 mass% and 15 mass% lignin, where the proton conductivity was seen to either increase (in the case of 5 mass% LMW and HMW lignin) or remain constant (in the case of 15 mass% LMW lignin). Surprisingly, 25LMW-SPEEK(80%) demonstrated a proton conductivity that was equivalent to that of the neat SPEEK and neat Nafion ionomers. This is quite impressive, given that 25% of the conductive SPEEK ionomer has been replaced with a bio-renewable polymer.

To gain insight into how the concentration of ions (both in the ionomer and in the adjacent solution) impact the ion permeability in these samples, the fixed charge group density $C_A^{m,w}$ was calculated from the IEC and EWU *via* the following equation: $C_A^{m,w} = (\text{IEC} \times \rho_w)/\text{EWC}$, where EWU is equilibrium water uptake (in grams of water per gram of dry polymer), and ρ_w is density of water (1 g cm^{-3}).[35] The fixed charge group density, combined with the total ion concentration of the external contiguous solution C_T^S, provides some information about the effect of Donnan exclusion on the ion transport in the ionomer.[36] Theoretically, at equilibrium, the ionizable sulfonic acid group of the ionomer nanocomposite requires an equivalent amount of counter-ions to balance the fixed charge groups, which results in unequal ion distribution between the membrane and the adjacent solution, leading to an electric potential that excludes the co-ions sorption, which is known as Donnan exclusion. Hence, calculating the total ion concentration of the external contiguous solution used for VO^{2+} permeability measurement can provide insight into the impact of Donnan exclusion on VO^{2+} transport, where the value of the total ion concentration in the external solution is $C_T^S = C_{SO_4^{2-}}^S = C_{VO^{2+},H^+}^S = 4.5$ mol L^{-1}.

The fixed charge group density $C_{SO_3^-}^{m,w}$ is calculated for each sample and summarized in Fig. 4. In general, the fixed charge group densities of all samples were higher than 4.5 mol L^{-1}, and the SPEEK(80%) series demonstrated lower fixed charge group density in general when compared with SPEEK(72%) series.

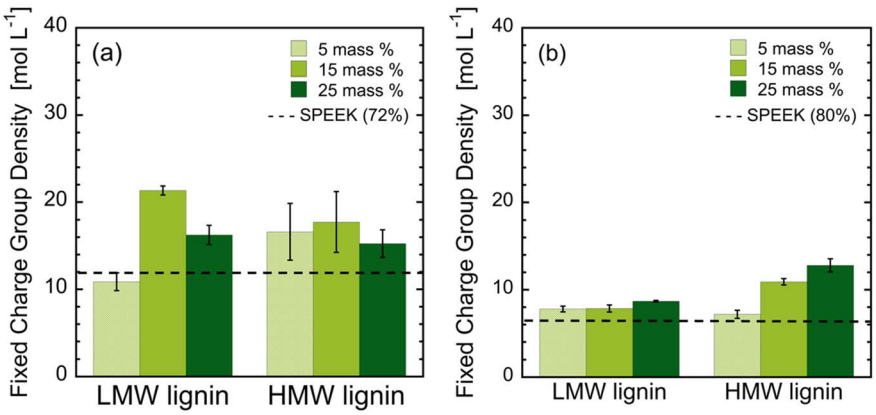

Fig. 4 Fixed group charge density for (a) SPEEK(72%) based nanocomposite membranes and (b) SPEEK(80%) based nanocomposite membranes. The dashed lines represent the average equilibrium water uptake and ion exchange capacity of neat SPEEK samples. Note, the error bars represent the standard deviation of the calculated averaged from measurements on at least three independent membranes.

This can be attributed to the higher equilibrium water uptake of the SPEEK with higher DS, which in turn, decreases the fixed charge group concentration. Additionally, though the SPEEK(80%) series shows fixed charge group density values larger than the external solution ion concentration, their $C^{m,w}_{SO_3^-}$ values are still closer to 4.5 mol L^{-1}, indicating the impact of Donnan exclusion on ion transport is negligible for these nanocomposites since most charge can be electrostatically balanced/screened by the counter-ions absorbed from the adjacent solution. Interestingly, SPEEK(72%) series membranes exhibit fixed charge group densities higher than 12 mol L^{-1}, with 15LMW-SPEEK(72%) and 15HMW-SPEEK(72%) presenting $C^{m,w}_{SO_3^-}$ values reaching 21 mol L^{-1} and 18 mol L^{-1}, respectively. This notably higher fixed charge group density of the membrane compared to the external ion concentration will lead to a larger Donnan potential, which could affect the transport of the positively charged VO^{2+}. Nevertheless, no correlation is observed between the high fixed charge group density and vanadium ion permeability, underscoring the fact that the transport of ions within the ionomer is affected by a multitude of different factors.

To elucidate the impact of the lignin dispersion state within these membranes on ion transport, transmission electron microscopy (TEM) was used to image the SPEEK–lignin composite membranes, where a dilute casting solution, with polymer concentration between 0.05 mass% to 0.1 mass%, was used to cast membranes directly on the copper grid that were thin enough to be successfully imaged *via* TEM. The results of this analysis are presented in **Fig. 5**. Specifically, Fig. 5a–c show the TEM images of SPEEK(72%) containing 5 mass%, 15 mass%, and 25 mass% LMW lignin, respectively, while Fig. 5d–f show the TEM of SPEEK(72%) containing 5 mass%, 15 mass%, and 25 mass% HMW lignin, respectively. The scale bars in all TEM images shown in Fig. 5 are identical and are equal to 600 nm. Note that equivalent TEM images for SPEEK(80%) containing 5 mass%, 15 mass%, and 25 mass% LMW and HMW lignins are shown in Fig. S6 in the ESI,† as the general dispersion states of lignin within this ionomer series are similar to their 3 h counterparts. Also note that TEM images of neat SPEEK(72%) and SPEEK(80%) are shown in Fig. S8.† As seen from the TEM images in Fig. 5, the dispersion state of lignin is highly variable, both with lignin concentration and lignin molecular weight. In general, the TEM images show a combination of small, well-dispersed lignin aggregates, as well as portions that contain large areas of a 'continuous' lignin phase. Nanocomposites containing 15 mass% LMW and HMW lignin demonstrated larger and more circular lignin aggregates when compared with samples containing 5 mass% and 25 mass% lignin, which provides some insight into the impact of the lignin dispersion state on VO^{2+} transport. Specifically, samples containing 15 mass% of lignin generally exhibit lower vanadium ion permeabilities compared with that of the samples containing 5 mass% and 25 mass% lignin as shown in Fig. 2. To ensure that the dispersion state observed at 15 mass% lignin was not an experimental error in TEM sample preparation or an artifact of image selective bias, additional TEM images of 15HMW-SPEEK(72%) are shown in Fig. S7 in the ESI.†

The presence of the uniformly dispersed lignin aggregates could lead to increased electrostatic interactions between the functional groups of lignin and the sulfonic acid groups of the SPEEK, where the presence of sulfonic acid, carboxylic acid, and hydroxyl groups contribute to the overall formation of the hydrophilic domains within the membrane. In general, the dispersion state of lignin did not appear to be significantly impacted by the molecular weight of the lignin, though the composites containing HMW lignin exhibited slightly larger lignin aggregates. One factor that plays an important role in tuning the dispersion state of the lignin is the functional group type and content. Modification (or addition) of functional groups on the surface of nanofillers is a common method leveraged to tune polymer–nanofiller interactions and obtain desired nanostructures and resulting membrane performances.[17,18,37]

As previously shown in Table 2, a larger content of guaiacyl hydroxyl groups and carboxylic acid groups are present in LMW lignin compared to the HMW lignin fraction (2.23 *vs.* 2.00 mmol

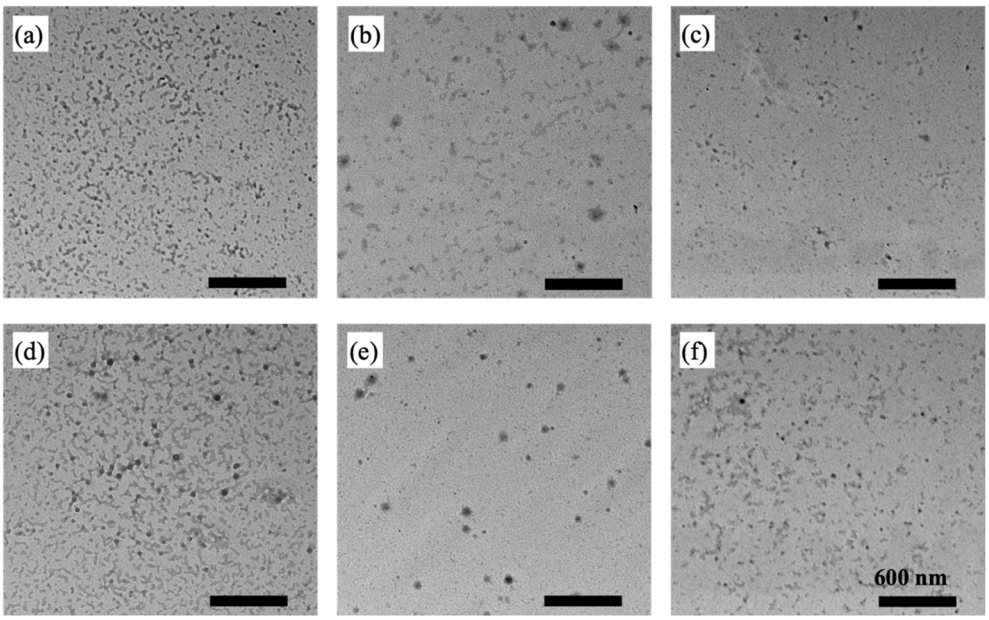

Fig. 5 Transmission electron microscopy (TEM) of SPEEK(72%) containing (a) 5 mass%, (b)15 mass%, and (c) 25 mass% LMW lignin and (d) 5 mass%, (e) 15 mass%, and (f) 25 mass% HMW lignin. Note, the scale bar in each image is 600 nm.

per gram of lignin for guaiacyl hydroxyl group and 0.59 *vs.* 0.45 mmol per gram of lignin for carboxyl acid group). This could provide some explanation as to the larger size of lignin aggregates in the HMW containing membranes. However, in general, both lignin fractions exhibited similar overall functional groups content, which may lead to the relatively similar dispersion states of lignin with different molecular weights (at a fixed lignin concentration). Further, we posit that at lower lignin concentrations, the abundant hydroxyl groups of the lignin interact with and act to modify the hydrophilic domains of the ionomer membranes. For both the LMW and HMW lignin, the total hydroxyl content is approximately 6.8 mmol per gram of lignin, which is more than three-fold higher than the content of sulfonic acid groups in SPEEK (1.57 mmol per gram of SPEEK). We believe that it is this interaction that results in the formation of more interconnected hydrophilic domains for proton transport, which ultimately leads to a higher proton conductivity. However, this synergistic effect diminishes at higher lignin loadings, especially for the SPEEK membranes containing HMW lignin (see Fig. 2b and d).

Considering the fabrication method used in this work for preparing lignin-SPEEK nanocomposite membranes (see Fig. 1 in the Experimental section), a discussion of the structure of lignin in solution is relevant and can provide some insight into the final lignin dispersion state in the solid ionomer composite membrane. All nanocomposite membranes were prepared *via* solution casting, where a casting solution containing both dissolved lignin and SPEEK was poured onto a quartz plate that was heated at 80 °C to allow for evaporation of the solvent, dimethylacetamide (DMAc). Therefore, the interactions among SPEEK, lignin, and DMAc in the casting solution will strongly affect the final lignin dispersion and aggregation within the dense ionomer membrane.[38–40] Along these lines, the aggregation of lignin in various solvents has been studied, including ionic liquids,[41–43] alkaline aqueous solutions,[44,45] and DMSO (both DMSO and DMAc are considered "good" solvents for lignin and SPEEK), where aggregation of lignin, captured *via* SANS, was observed in all solvents investigated.[38] Though, to the best of our knowledge, this is the first time the aggregation of lignin within a dense polymer membrane has been captured and investigated. It has been proposed that various forces are responsible for lignin aggregation in solution, where the intermolecular hydrogen bonds and noncovalent π–π interactions between phenyl rings are the predominant forces that hold lignin subunits together, leading to lignin aggregates in organic solvents like DMSO and DMAc. Interestingly, work from Kubo and Kadla,[46] indicated that stronger hydrogen bonding (H-bonding) occurs between the aliphatic hydroxyl compared to those found on phenolic rings, which was confirmed by the aforementioned SANS study where the degree of lignin aggregation in DMSO was found to be proportional to the content of aliphatic hydroxyl groups.[38]

As seen in Fig. 6a and b, lignin aggregation was observed for SPEEK–lignin ionomer composites, irrespective of the lignin MW, where Fig. 6a and b show SPEEK containing 5 mass% LMW and HMW lignins, respectively. The similar aggregation observed for both the LMW and HMW lignins may be attributed to the fact that the total hydroxyl group contents for both fractions are similar. It should be noted that the sulfonic acid groups of the SPEEK form hydrogen bonds with lignin, while simultaneously, the lignin forms intermolecular hydrogen bonds with itself. The former restricts the aggregation of lignin, while the latter acts to hold lignin subunits together. Hence, with the evaporation of DMAc solvent during casting, these opposing intermolecular interactions further affect the lignin dispersion state in the ionomer matrix. Ultimately, as seen from

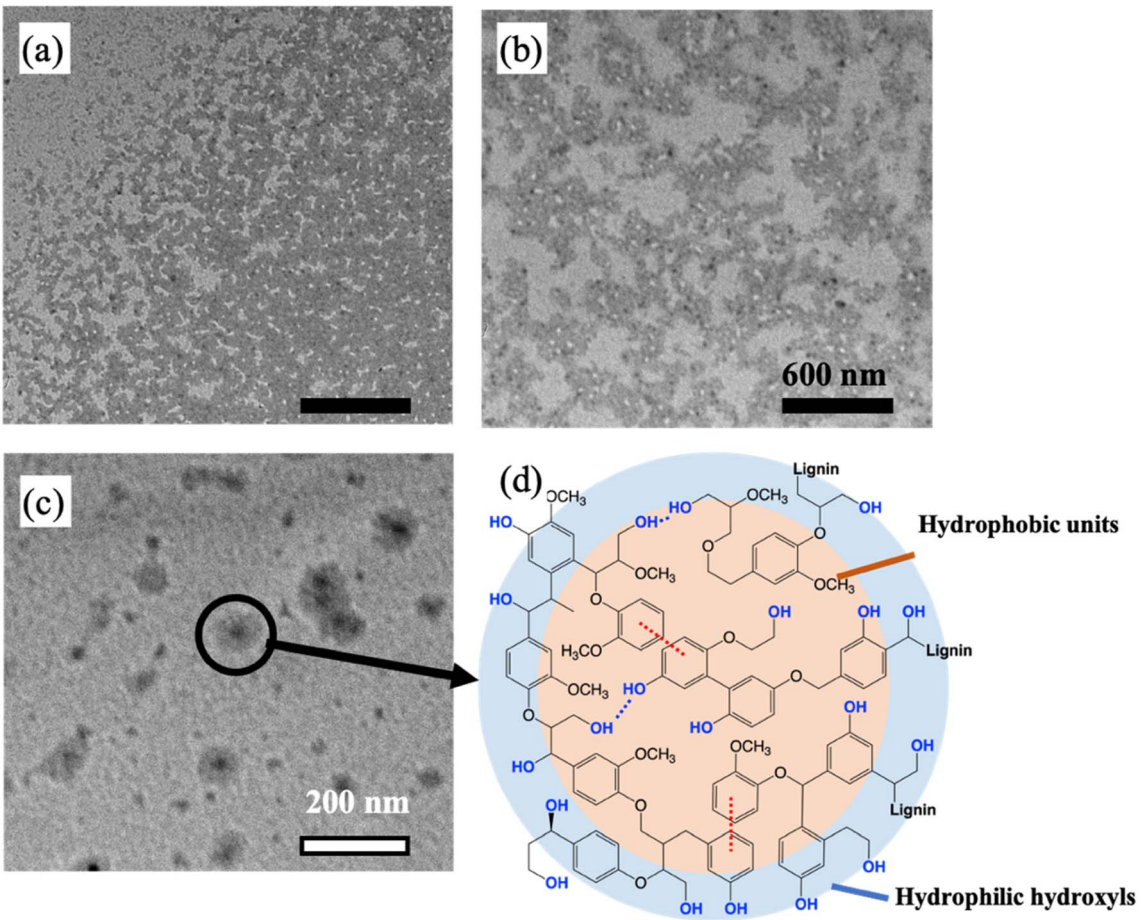

Fig. 6 Transmission electron microscopy (TEM) images of SPEEK(72%) containing (a) 5 mass% LMW lignin, (b) 5 mass% HMW lignin, and (c) 15 mass% LMW lignin. Note, black scale bars for (a) and (b) are equal to 600 nm, while the white scale bar for (c) is equal to 200 nm. (d) Illustrative schematic of the "core–shell" structure of lignin aggregates in SPEEK, intermolecular π– π interactions and hydrogen bonds are represented by red and blue dotted lines, respectively.

the TEM images in Fig. 5 and **6** (for example, Fig. 5a *vs.* 6a), the 'competitive' hydrogen bond formation leads to both a uniformly dispersed lignin phase, as well as larger, more continuous lignin phase/lignin agglomerations.

As mentioned above, nanocomposites containing 15 mass% LMW and HMW lignins demonstrated larger and more circular lignin aggregates when compared with samples containing 5 mass% and 25 mass% lignin (see Fig. 5). When these circular-like aggregates are viewed under higher magnification (Fig. 6c), a "core–shell" structure can be observed, where a dark black core (on the order 10 nm) is surrounded by a more diffuse, lighter grey shell (total core–shell diameter on the order of 100 nm). An illustrative schematic of this lignin aggregation phenomenon is presented in Fig. 6d, where the abundant hydroxyl groups decorating the lignin form an outer hydrophilic shell, while the phenolic rings form an inner hydrophobic core. Note that in Fig. 6d, the dashed red lines represent noncovalent π–π interactions, while the dashed blue lines represent H-bonding. This "nano-segregated" hydrophilic–hydrophobic core–shell structure has been previously observed during the preparation of lignin nanoparticles,[9,47,48] though this is the first time this type of core–shell lignin structure has been observed within a solid polymer matrix.

To improve our understanding of the nanostructure of these membranes, and further elucidate the interplay between structure and membrane performance properties, structural characterization of the hydrated SPEEK–lignin composite membranes was carried out *via* SANS. The results of this characterization are shown in Fig. 7. Note, all membranes were soaked in D_2O for at least 48 h prior to SANS experiments, and all SANS experiments were performed at room temperature (≈293 K). It should also be noted that while SANS and small-angle X-ray scattering (SAXS) have been used to characterize the phase segregated structure of SPEEK, the resulting scattering spectra are quite different.[33,49–51] This difference is primarily due to the different membrane preparation conditions, as well as the variety of fabrication routes used to obtain SPEEK. For example, post sulfonation of PEEK and direct polymerization of sulfonated monomers can result in SPEEK with different sulfonic acid groups distributions along the aromatic backbone, which can significantly alter the nanostructure of the sulfonated ionomer, and ultimately, the final performance properties of the ionomer. This concept was

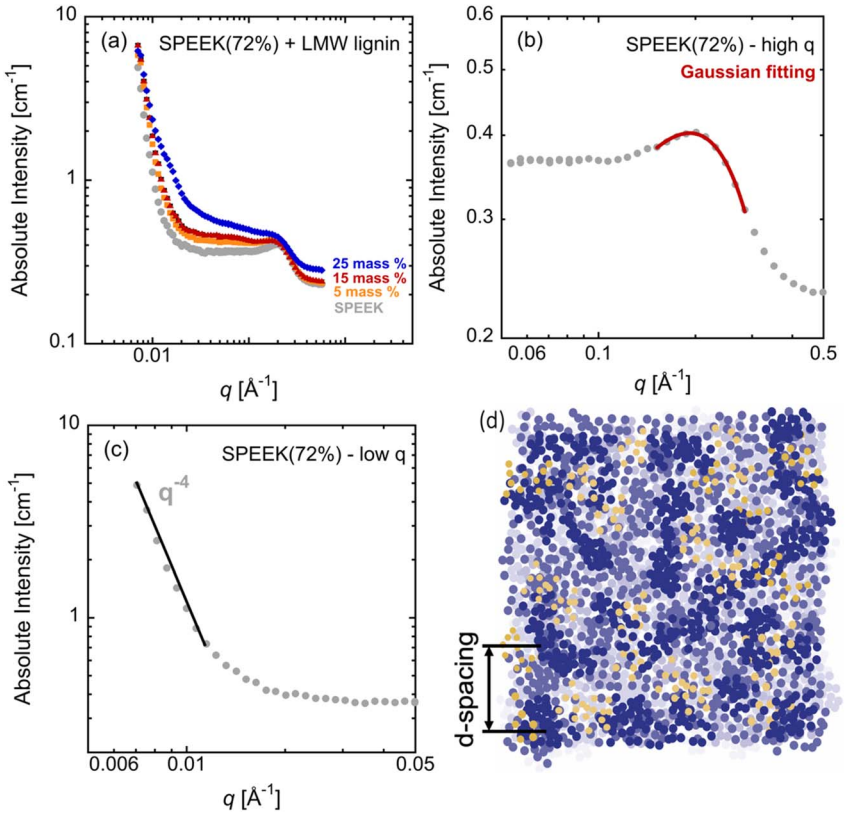

Fig. 7 (a) SANS spectra of SPEEK(72%) (closed gray circles) and SPEEK(72%) containing 5 mass% (closed orange squares), 15 mass% (closed red triangles), and 25 mass% (closed blue diamonds) LMW lignin. (b) SANS spectrum of the high-q region for SPEEK(72%), along with the Gaussian fitting of the ionomer peak (solid red line). (c) SANS spectrum of the low-q region for SPEEK(72%). The solid black line indicates that as the intensity decays following q^{-4}. (d) Illustrative schematic of hydrophilic domains of hydrated SPEEK membrane, where only water molecules (blue dots) and sulfonic acid groups (yellow dots) are shown. Note that the various shades of the blue dots have been employed to demonstrate depth within the membrane.

recently highlighted when researchers created both "random" and "blocky" SPEEK and observed significantly higher proton conductivity, at the same sulfonic acid content, for their block SPEEK membranes.[29]

The full SANS spectra of SPEEK(72%) and LMW lignin-containing composites are shown in Fig. 7a. As seen in Fig. 7a, there are two distinct features present in all scattering curves: (1) a scattering peak at high q ($q \approx 0.2$ Å^{-1}) and (2) a low-q upturn, which have been highlighted for SPEEK(72%) in Fig. 7b and c, respectively. We will discuss the low-q uptrun behavior of the SANS data in more detail later in this section. For ionomer membranes, the peak at high q has been assigned to the spacing between (center-to-center distance) hydrophilic domains in the hydrated membranes and is oftentimes referred to as the "ionomer" or "hydrophilic" peak.[49,52] Note that the full collection of high-q SANS spectra (*i.e.*, the ionomer region) for both the SPEEK(72%) and SPEEK(80%) series can be found in Fig. S9 in the ESI.† For ionomers, such as Nafion, distinct nanophase separation of the hydrophobic PTFE-like backbone and the terminal hydrophilic sulfonic acid groups occurs upon hydration, leading to locally-flat hydrophilic domains surrounded by a semi-crystalline polymer matrix.[53,54] However, unlike Nafion, the hydrophilic sulfonic acid groups in SPEEK are directly tethered on the aromatic backbone, which can lead to weaker nanophase separation upon hydration. That is, the interface between the ionic domains embedded in the hydrophobic matrix is less distinct, a feature which has captured with computational modeling of ionomers with similar architectures.[55,56] This has been illustrated in the schematic shown in Fig. 7d.

To have a more quantitative analysis of the SANS curves, the ionomer peaks were fit to a Gaussian function (see Section 4 in the ESI†). Briefly, the Bragg approximation was used to determine the location of the ionomer peak for each composite, where the wave vector of the ionomer peak can be correlated to Bragg d-spacing *via* the equation: d-spacing $\approx 2\pi/q$.[17,57,58] In addition to the periodic spacing between hydrophilic domains, the spread (or breadth) of the ionomer peak was represented by the standard deviation of the Gaussian fitting (Gaussian root mean square width, σ) for each sample. The results of this analysis are presented in Fig. 8. Note, the dashed line in each figure represents that respective value for neat SPEEK membranes. As seen in Fig. 8a and b, the d-spacing of SPEEK(72%) and SPEEK(80%) are 3.3 nm and 3.3 nm, respectively, indicating that the spacing between hydrophilic domains is quite similar for both SPEEK(72%) and SPEEK(80%)

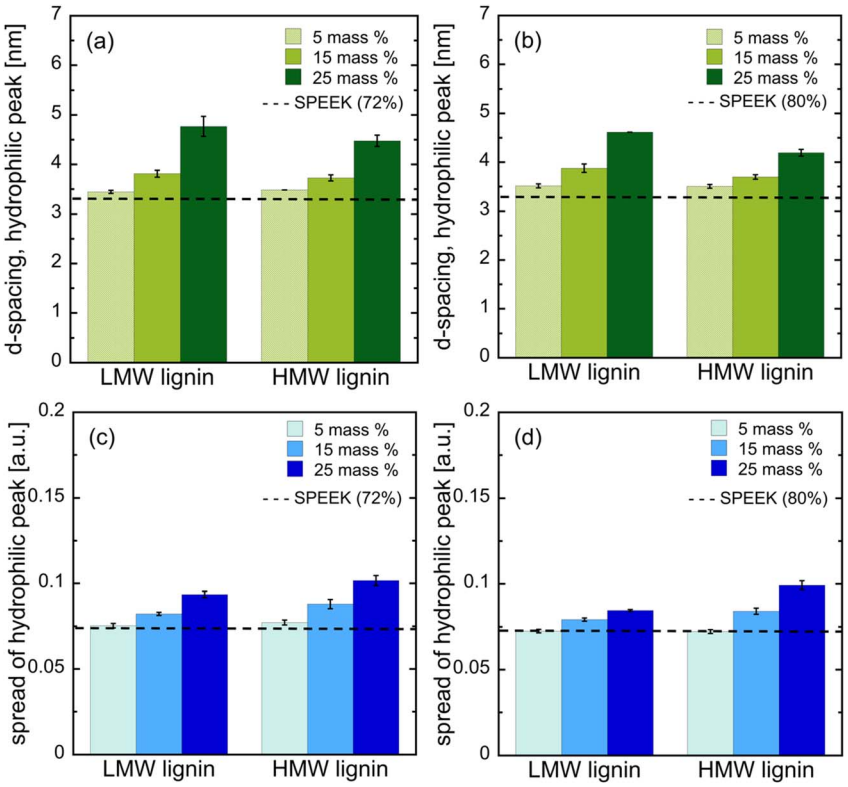

Fig. 8 *d*-spacing (in nm) for (a) SPEEK(72%) containing LMW and HMW lignin at 5 mass%, 15 mass% and 25 mass% loading; (b) SPEEK(80%) containing LMW and HMW lignin at 5 mass%, 15 mass% and 25 mass% loading. Spread of the ionomer peak of (c) SPEEK(72%) lignin containing films; and (d) SPEEK(80%) lignin containing films. The spread of hydrophilic peak for each sample is represented by the standard deviation of the Gaussian fitting (Gaussian root mean square width, σ), and the dash line in each figure represents the data of neat SPEEK films. The error bars in each figure were obtained from the Gaussian regression.

membranes. With respect to ion transport, these similar *d*-spacing values are consistent with the proton conductivity data for these two ionomers with similar proton conductivities ($\approx$100 mS cm^{-1}). Furthermore, the *d*-spacing increased with increased lignin loading.

The most pronounced increase in *d*-spacing observed for SPEEK membranes containing 25 mass% lignin (both LMW and HMW lignin). For example, from Fig. 8a, the *d*-spacing is seen to increase from approximately 3.4 nm (for SPEEK(72%)) to 4.9 nm (for 25LWM-SPEEK(72%)), an over 40% increase in spacing of the hydrophilic domains. This increase in *d*-spacing is more likely caused by an increase in the hydrophobic portion of the lignin-containing composite, which has been induced by the introduction of lignin, a (relatively) hydrophobic polymer. This significant increase in *d*-spacing of the ionic domains may help explain the approximate 25% reduction in proton conductivity measured for these membranes (100 mS cm^{-1} *vs.* 75 mS cm^{-1}), as the spacing between proton 'hopping' sites has increased as well as water uptake has been reduced with 25 mass% lignin incorporated, leading to reduced proton transport *via* vehicular mechanism. However, as seen from Fig. 2c and f, the proton selectivities of all SPEEK–lignin composite ionomers were higher than that of both neat SPEEK and Nafion. This result implies that changes to the nanostructure of the SPEEK with the introduction of lignin have a greater impact on the vanadium ion permeability than on the overall proton conductivity of these membranes.

We note that this result may also be related to the difference in the overall size of the hydrated diffusants sizes as well. Vanadium ions exist in a hydrated form in aqueous solutions, with an approximate size of 6 Å, while the size of hydrated protons (*i.e.*, hydronium ions) is approximately 1 Å.[59] In addition to the change in spacing of the ionic domains with the introduction of lignin, the impact of lignin on the width of the ionomer peak is highlighted in Fig. 8c and d for SPEEK(72%)-based and SPEEK(80%)-based ionomers, respectively. Changes of peak width indicates the distribution in values of *d*-spacing of the ionic domains. That is, an increase in the breadth of the ionomer peak would imply an increase in the spread (or standard deviation) of the average value of *d*-spacing of the ionic domains. Similar to what is observed with the *d*-spacing data, the breadth is seen to increase with increased lignin loading for both SPEEK(72%)-based and SPEEK(80%)-based membranes, with the most noticeable increase observed for ionomers containing 25 mass% LMW and HMW lignin.

The presence of a low-*q* upturn in the SANS data can provide information regarding the impact of lignin on the interfacial properties of the hydrophobic and hydrophilic regions of the ionomer. The *q*-dependence of the low-*q* SANS data is shown in

Fig. 9. Specifically, following power law equation was regressed to the low-q data

$$I(q)=(\text{scale})q^{\alpha} + \text{background} \quad (5)$$

where the scale and α, the power law exponent, are unitless fitting parameters. The background was fixed to the value from the flat part of the scattering curve. As seen from Fig. 9a and b, the values of the power law exponent for SPEEK(72%) and all SPEEK(72%) membranes containing LMW lignin were either approximately -3 or -4. However, when looking at this low-q behavior for SPEEK(80%) membranes (Fig. 9c and d), we observe that the value of power law exponent for all membranes was approximately -3. The first thing to note is that this low-q upturn is present in ionomer membranes containing no lignin, indicating that this behavior is inherent to the neat SPEEK and is not caused by the addition of lignin to the ionomer. This low-q upturn behavior has been observed in the SAS data of several sulfonic acid-based membranes, including both Nafion and SPEEK, where researchers have observed exponents ranging from approximately -4 to -2.[25,49,60] While this q^{-4} decay is observed at lower wave vectors than those of the ionomer peak itself, the q^{-4} upturn has been attributed to sharp boundary between two immiscible phases,[61,62] suggesting sharp interface between hydrophobic and hydrophilic (water containing) domains.[63,64] A transition from q^{-4} to q^{-3} behavior in this low-q region could be caused by several factors, such as rough or irregular surfaces or long-range structural correlations. However, to date, this q^{-3} decay has been attributed to rough interfaces (or less distinct phase separation) within nanophase segregated ionomer membranes.[60,65,66] Of note, some researchers have overserved a q^{-2} dependence in the low-q SAS data of SPEEK, which was attributed to the inherent lamellae structure of the SPEEK. However, as seen in Fig. 9, this dependence in the low-q data was not observed for any membranes in this study.[49]

As seen in Fig. 9, only neat SPEEK(72%) and SPEEK(72%) membranes containing LMW lignin, specifically 5LMW-SPEEK(72%) and 15LMW-SPEEK(72%), demonstrated a q^{-4} decrease in scattering intensity (Porod scattering) in this low-q regime of the SANS spectra, suggesting that, in general, the SPEEK(72%)-based membranes containing LMW lignin exhibited a sharp, distinct interface (or separation) between interconnected hydrophilic, ionic domains and hydrophobic, aromatic domains. However, for 25LMW-SPEEK(72%) (Fig. 9b), as well as for all HMW lignin concentrations (Fig. 9c and d), a q^{-3} decrease in the low-q intensity was observed. When

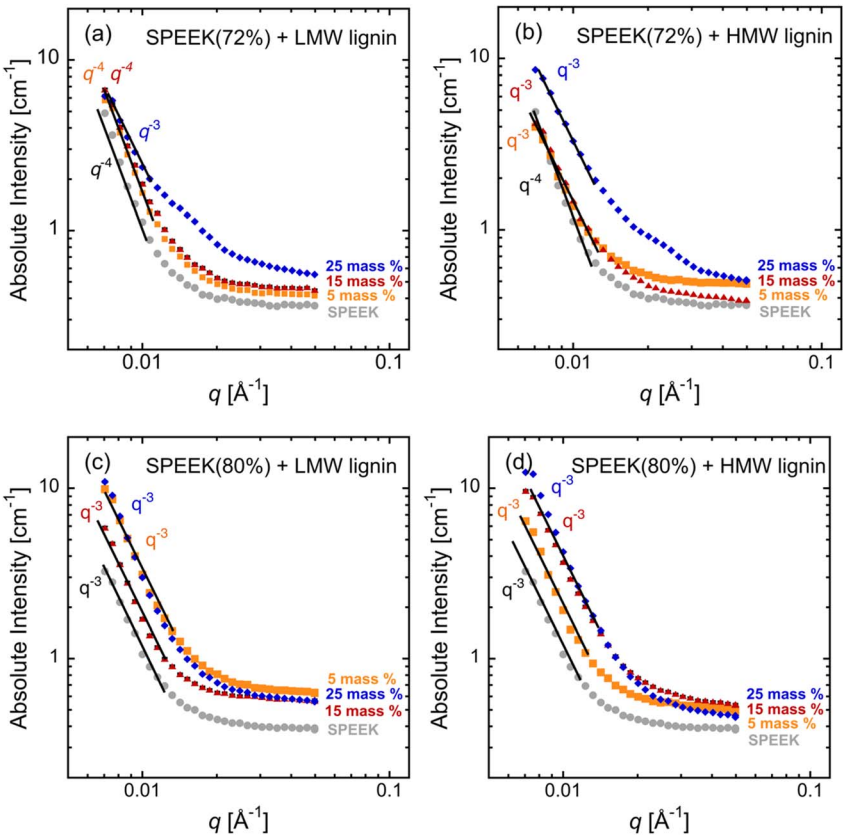

Fig. 9 Low-q region of SANS curves for SPEEK(72%) containing (a) 0 mass% (solid gray circles), 5 mass% (solid orange squares), 15 mass% (solid red triangles), and 25 mass% (solid blue diamonds) LMW lignin and (b) 0 mass% (solid gray circles), 5 mass% (solid orange squares), 15 mass% (solid red triangles), and 25 mass% (solid blue diamonds) HMW lignin. Low-q region of SANS curves for SPEEK(80%) containing (c) 0 mass% (solid gray circles), 5 mass% (solid orange squares), 15 mass% (solid red triangles), and 25 mass% (solid blue diamonds) LMW lignin and (d) 0 mass% (solid gray circles), 5 mass% (solid orange squares), 15 mass% (solid red triangles), and 25 mass% (solid blue diamonds) HMW lignin.

considered alongside the observed proton conductivity (Fig. 2b and e), the q^{-3} is most likely representative of a rough interface, indicating less distinct phase separation between the hydrophilic and hydrophobic domains of the ionomer.[65–67] Of note, the structure of hydrated SPEEK was recently investigated using SAXS, in which a q^{-4} behavior in the SANS data on the high-q side of the ionomer peak ($q > 0.1$ Å^{-1}) was observed.[58] However, due to the small change in scattering intensity of the SANS data over the equivalent q regime, we were unable to obtain meaningful information from such an analysis.

There are several interesting insights that these results provide regarding the proton conductivities of these membranes. First, the introduction of HMW lignin results in ionomer composites with decreased phase separation, for both SPEEK(72%) and SPEEK(80%) membranes. This is most notable for the SPEEK(72%) series, as prior to the introduction of HMW lignin, the SPEEK(72%) membrane exhibited a q^{-4} decrease in the low-q SANS data (Fig. 9b), which again, is indicative of a sharp, distinct interface between the hydrophilic and hydrophobic domains within the nanophase segregated ionomer. However, as seen in Fig. 9c and d, the q^{-3} decrease in scattering intensity in this low-q regime of the SANS spectra was seen for SPEEK(80%) and SPEEK(80%) containing either LMW and HMW lignin. Second, for the SPEEK(72%) series containing LMW lignin, a transition from a sharp/smooth to rough interface between the hydrophilic and hydrophobic domains is observed when the LMW lignin concentration is increased from 15 mass% to 25 mass%, where a transition from q^{-4} to q^{-3} behavior is observed.

This may help to explain why the proton conductivities of the SPEEK(72%)-based membranes were greater than or similar to that of their SPEEK(80%)-based counterparts, with the exception of membranes containing 25 mass% LMW lignin (Fig. 2b *vs.* e; 25LMW-SPEEK(72%) *vs.* 25LMW-SPEEK(80%)). Theoretically, enhanced phase separation is anticipated with increased content of charged groups. However, while the SPEEK(80%) had a higher DS, the sulfonic acid groups were distributed along the aromatic backbone in such a way that it resulted in similar phase separation as SPEEK(72%), and thus, conductivities that were similar to the SPEEK(72%) membranes with a lower DS. Further, the sharp interface of the SPEEK(72%)-based ionomers containing LMW lignin may also help to explain why the proton selectivities of these membranes were higher than their SPEEK(80%)-based counterparts, with again, the exception of those membranes containing 25 mass% LMW lignin (Fig. 2c *vs.* f; 25LMW-SPEEK(72%) *vs.* 25LMW-SPEEK(80%)).

Based on the observe increased proton conductivity and simultaneous decrease in EWU and IEC, along with the other results reported above, illustrative schematics of the ionic network for the neat SPEEK and SPEEK–lignin ionomer biocomposites, which demonstrated this improved performance, are provided in Fig. 10. As seen in Fig. 10, the higher values of EWU and IEC with lower proton conductivity observed for neat SPEEK can be explained by a larger concentration of "dead ends" or an increased tortuosity of the ionic channels, or some combination of both. That is, while there is greater access to sulfonic acid groups, and thus, higher values of water uptake (and higher values of IEC), the degree of percolation of these ionic channels across the membrane is lower. However, with the introduction of lignin, up to a concentration of 15 mass%, the hydrophilic channels for ion and water transport become more interconnected, leading to a decrease in overall tortuosity of the ionic channels and a decrease in the overall concentration of ionic groups forming these ionic channels. This provides a reasonable interpretation of the observed properties, that is, a simultaneous increase in proton conductivity and decrease in EWU and IEC.

Finally, to test the viability of these SPEEK–lignin membranes as potential PEMs for energy storage devices, such as the redox flow battery, routine battery testing was performed on VRFBs with one SPEEK (SPEEK(72%)) and one SPEEK–lignin (15LMW-SPEEK(72%)) membrane. Charge–discharge cycling was performed at 20 mA cm^{-2} over a voltage range of 1.0 to 1.8 V until the discharge curves stabilized. Next, polarization curves were developed on fully charged RFBs with each membrane and the voltage and power density as a function of current density are shown in Fig. 11a and b, respectively. As shown in Fig. 11a, the

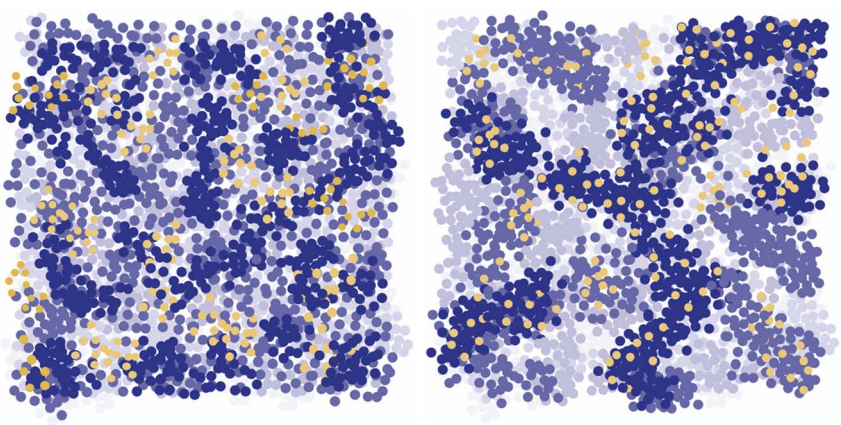

Fig. 10 Illustrative schematic of the difference in ionic network structure (hydrophilic channels) of neat SPEEK (left) *vs.* the SPEEK–lignin ionomer biocomposite (right) membranes. Only water molecules (blue dots) and sulfonic acid groups (yellow dots) are shown to highlight the hydrophilic channels for ions and water transport. Note that the various shades of the blue dots have been employed to demonstrate depth within the membrane.

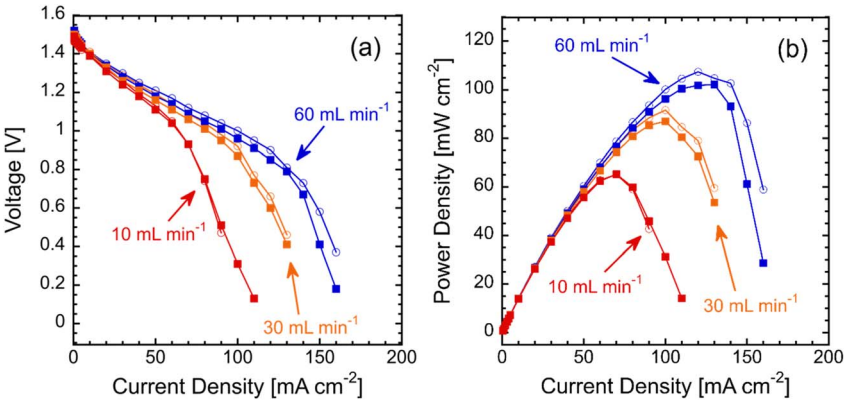

Fig. 11 Electrochemical performance of VRFBS with SPEEK(72%) (open circles) and 15LMW–SPEEK(72%) (filled squares) membranes. (a) Polarization curves, voltage output with increasing current density, for electrolyte flow rates of 10 mL min^{-1} (red), 30 mL min^{-1} (orange), and 60 mL min^{-1} (blue) and (b) corresponding power density *vs.* current density. Note that the voltage outputs are not *iR*-corrected and the electrolyte is 1.0 M V in 3.0 M H_2SO_4.

discharge voltage (non *iR*-corrected) is similar for each RFB regardless of the membrane type, and the voltage output increases with electrolyte flow rate through the cell. The increase in discharge voltage at higher flow rates is typical for flow batteries because the electrode channels maintain a higher concentration of active species. A similar concentration polarization resistance (rapid decrease in voltage at high current density) is observed as the electrodes and electrolyte are the same in each cell. Importantly, the ohmic polarization, which determines the linear drop (slope of the plateau) in the discharge curve, is identical in each cell. As this is a function of the electrical and ionic resistance, and the electrical resistance is small (also equivalent across cells), the ionic resistance/transport through each membrane must also be equal. This result is consistent with the proton conductivity measured for each membrane, where, as seen in Fig. 2b, there is no measurable difference in this value between the neat SPEEK and that containing 15 mass% LMW lignin (both were ~100 mS cm^{-1}). The slight difference in polarization curves can then be attributed to a slight change in activation polarization. However, this small difference may also be a result of simple experimental variation.

Finally, Fig. 11b shows the power density, which is the product of the current density and voltage output, as a function of current density for various electrolyte flow rates. As seen from this figure, at a given electrolyte flow rate, the performance of each membrane is similar. This is expected given the similarities in the polarization curves observed in Fig. 11a. The peak power density of 107 mW cm^{-2} in cells with SPEEK(72%) is only slightly higher than that with 15LMW-SPEEK(72%) (102 mW cm^{-2}). However, we note that these values of the peak power density are both notably lower than a RFB operated with the benchmark ionomer, Nafion 117 (~140 mW cm^{-2}). Further, the authors note that a more comprehensive investigation on the RFB performance of these membranes, including characterizing their oxidative stability, is needed and is currently the focus of ongoing work. Nonetheless, these results suggest that more sustainable, lignin-containing ionomer composites may provide suitable membranes for large-scale redox flow batteries.

4 Conclusions

In summary, we have reported a series of sulfonated ionomer nanocomposites containing cleaned and fractionated lignin, of both low and high MWs, that demonstrated significantly reduced vanadium ion permeability, and in some cases, enhanced proton conductivities, leading to markedly improved proton selectivity of our SPEEK–lignin hybrid composites. Most notably, 15HMW-SPEEK(80%) exhibited proton selectivities that were an order of magnitude higher than neat SPEEK and approximately six-fold higher than the current benchmark ionomer, Nafion. Further, analysis of the SANS spectra of the ionomer composites indicated that the degree of phase separation was dictated by both the DS of the SPEEK and the MW of the lignin. When employed in VRFBs, 15LMW-SPEEK(72%) demonstrates a sustainable alternative to traditional ionomer membranes, with a peak power over 100 mW cm^{-2} at discharge currents above 130 mA cm^{-2}. When compared to Nafion, the current benchmark ionomer membrane for VRFBs, a notebook sheet-sized membrane of our SPEEK–lignin composite is over an order of magnitude cheaper (~\$120 *vs.* ~\$5), all while replacing 25% of the petroleum-based SPEEK with bio-renewable lignin. Despite the concise and straightforward membrane fabrication process for these nanocomposite membranes, the demonstrated approach of using renewably processed and fractionated lignin in conjunction with a cost-effective sulfonated ionomer provides insight for designing proton exchange membranes with better performance properties and at a lower cost, improving the viability of wide-scale adoption of grid-scale energy storage technologies like the redox flow battery.

Data availability

The data that support the findings of this study can either be found in the supplementary documents or are available from the corresponding author upon reasonable request.

Author contributions

Xueting Wang: formal analysis, investigation, writing – original draft, visualization. Mayura Silva: investigation, writing – review & editing. Colleen Clarke: investigation, writing – review & editing. Bronson Lynn: investigation, writing – review & editing. Mark Robertson: investigation, writing – review & editing. Aidan J. Leopold: investigation. Oreoluwa Agede: investigation, writing – review & editing. Lilin He: investigation, writing – review & editing. Stephen Creager: writing –review & editing. Mark E Robets: formal analysis, writing – review & editing, supervision. Mark C. Thies: writing – review & editing. Eric M. Davis: conceptualization, validation, writing – review & editing, supervision.

Conflicts of interest

The authors declare that they have no known competing financial interests or personal relationships that could have appeared to influence the work reported in this paper.

Acknowledgements

This material is based upon work supported by the National Science Foundation under Grant No. DMR-1848347, CBET-1915787, and CBET-1725919. The authors would like to thank Dr Zachariah Pittman for his help with the molecular weight characterization of all lignin samples. This research used resources at the High Flux Isotope Reactor, a DOE Office of Science User Facility operated by the Oak Ridge National Laboratory. The beam time was allocated to CG2 on proposal number IPTS-30030.1.

References

1 A. Castillo and D. F. Gayme, Grid-Scale Energy Storage Applications in Renewable Energy Integration: A Survey, *Energy Convers. Manage.*, 2014, **87**, 885–894, DOI: **10.1016/j.enconman.2014.07.063**.

2 Y. Shi, C. Eze, B. Xiong, W. He, H. Zhang, T. M. Lim, A. Ukil and J. Zhao, Recent Development of Membrane for Vanadium Redox Flow Battery Applications: A Review, *Appl. Energy*, 2019, **238**, 202–224, DOI: **10.1016/j.apenergy.2018.12.087**.

3 A. H. Avci, D. A. Messana, S. Santoro, R. A. Tufa, E. Curcio, G. Di Profio and E. Fontananova, Energy Harvesting from Brines by Reverse Electrodialysis Using Nafion Membranes, *Membranes*, 2020, **10**(8), 168, DOI: **10.3390/membranes10080168**.

4 G. Hernández-Flores, H. M. Poggi-Varaldo and O. Solorza-Feria, Comparison of Alternative Membranes to Replace High Cost Nafion Ones in Microbial Fuel Cells, *Int. J. Hydrogen Energy*, 2016, **41**(48), 23354–23362, DOI: **10.1016/j.ijhydene.2016.08.206**.

5 H. Zhu, SPEEK Scaling UP, *Joule*, 2022, **6**(4), 718–720, DOI: **10.1016/j.joule.2022.03.006**.

6 B. G. Thiam, A. El Magri and S. Vaudreuil, An Overview on the Progress and Development of Modified Sulfonated Polyether Ether Ketone Membranes for Vanadium Redox Flow Battery Applications, *High Perform. Polym.*, 2022, **34**(2), 131–148, DOI: **10.1177/09540083211049317**.

7 R. Jia, C. He, Q. Li, S.-Y. Liu and G. Liao, Renewable Plant-Derived Lignin for Electrochemical Energy Systems, *Trends Biotechnol.*, 2022, **40**(12), 1425–1438, DOI: **10.1016/j.tibtech.2022.07.017**.

8 N. Gregorich, J. Ding, M. C. Thies and E. M. Davis, Novel Composite Hydrogels Containing Fractionated, Purified Lignins for Aqueous-Based Separations, *J. Mater. Chem. A*, 2021, **9**(2), 1025–1038, DOI: **10.1039/D0TA09046H**.

9 D. Tian, J. Hu, J. Bao, R. P. Chandra, J. N. Saddler and C. Lu, Lignin Valorization: Lignin Nanoparticles as High-Value Bio-Additive for Multifunctional Nanocomposites, *Biotechnol. Biofuels*, 2017, **10**(1), 192, DOI: **10.1186/s13068-017-0876-z**.

10 J. Ye, D. Yuan, M. Ding, Y. Long, T. Long, L. Sun and C. Jia, A Cost-Effective Nafion/Lignin Composite Membrane with Low Vanadium Ion Permeation for High Performance Vanadium Redox Flow Battery, *J. Power Sources*, 2021, **482**, 229023, DOI: **10.1016/j.jpowsour.2020.229023**.

11 J. Ye, X. Lou, C. Wu, S. Wu, M. Ding, L. Sun and C. Jia, Ion Selectivity and Stability Enhancement of SPEEK/Lignin Membrane for Vanadium Redox Flow Battery: The Degree of Sulfonation Effect, *Front. Chem.*, 2018, **6**, 549, DOI: **10.3389/fchem.2018.00549**.

12 J. Ye, Y. Cheng, L. Sun, M. Ding, C. Wu, D. Yuan, X. Zhao, C. Xiang and C. Jia, A Green SPEEK/Lignin Composite Membrane with High Ion Selectivity for Vanadium Redox Flow Battery, *J. Membr. Sci.*, 2019, **572**, 110–118, DOI: **10.1016/j.memsci.2018.11.009**.

13 Y. Pu, S. Cao and A. J. Ragauskas, Application of Quantitative 31P NMR in Biomass Lignin and Biofuel Precursors Characterization, *Energy Environ. Sci.*, 2011, **4**(9), 3154, DOI: **10.1039/c1ee01201k**.

14 Y.-Y. Wang, M. Li, C. E. Wyman, C. M. Cai and A. J. Ragauskas, Fast Fractionation of Technical Lignins by Organic Cosolvents, *ACS Sustainable Chem. Eng.*, 2018, **6**(5), 6064–6072, DOI: **10.1021/acssuschemeng.7b04546**.

15 J. Chen, F. Shen, G. Lyu, G. Yang, N. Lu and C. Hu, Structural Characterization of Lignin from Native, Kraft and Soda-AQ Pulping of Pennisetum Sinese Roxb. (P. Sinese), *Cellul. Chem. Technol.*, 2018, **52**(5–6), 371–380.

16 A. Adjaoud, R. Dieden and P. Verge, Sustainable Esterification of a Soda Lignin with Phloretic Acid, *Polymers*, 2021, **13**(4), 637, DOI: **10.3390/polym13040637**.

17 D. Allison, X. Wang, M. S. Silva, S. Creager, T. B. Martin and E. M. Davis, Role of Nanoparticle Size and Surface Chemistry on Ion Transport and Nanostructure of Perfluorosulfonic Acid Ionomer Nanocomposites, *Soft Matter*, 2022, **18**, 3342–3357, DOI: **10.1039/D1SM01573G**.

18 A. Domhoff, A. Balwani, T. B. Martin and E. M. Davis, Leveraging Nanoparticle Dispersion State To Tune Vanadium Ion Selectivity of Nanophase-Segregated Ionomer Nanocomposites for Redox Flow Batteries, *ACS*

Appl. Energy Mater., 2019, **2**(12), 8535–8549, DOI: **10.1021/acsaem.9b01443**.

19 S. Bukola, Y. Liang, C. Korzeniewski, J. Harris and S. Creager, Selective Proton/Deuteron Transport through Nafion|Graphene|Nafion Sandwich Structures at High Current Density, *J. Am. Chem. Soc.*, 2018, **140**(5), 1743–1752, DOI: **10.1021/jacs.7b10853**.

20 S. Liu, L. Wang, Y. Ding, B. Liu, X. Han and Y. Song, Novel Sulfonated Poly (Ether Ether Keton)/Polyetherimide Acid-Base Blend Membranes for Vanadium Redox Flow Battery Applications, *Electrochim. Acta*, 2014, **130**, 90–96, DOI: **10.1016/j.electacta.2014.02.144**.

21 W. T. Heller, M. Cuneo, L. Debeer-Schmitt, C. Do, L. He, L. Heroux, K. Littrell, S. V. Pingali, S. Qian, C. Stanley, V. S. Urban, B. Wu and W. Bras, The Suite of Small-Angle Neutron Scattering Instruments at Oak Ridge National Laboratory, *J. Appl. Crystallogr.*, 2018, **51**(2), 242–248, DOI: **10.1107/S1600576718001231**.

22 W. T. Heller, J. Hetrick, J. Bilheux, J. M. B. Calvo, W.-R. Chen, L. DeBeer-Schmitt, C. Do, M. Doucet, M. R. Fitzsimmons, W. F. Godoy, G. E. Granroth, S. Hahn, L. He, F. Islam, J. Lin, K. C. Littrell, M. McDonnell, J. McGaha, P. F. Peterson, S. V. Pingali, S. Qian, A. T. Savici, Y. Shang, C. B. Stanley, V. S. Urban, R. E. Whitfield, C. Zhang, W. Zhou, J. J. Billings, M. J. Cuneo, R. M. F. Leal, T. Wang and B. Wu, Drtsans: The Data Reduction Toolkit for Small-Angle Neutron Scattering at Oak Ridge National Laboratory, *SoftwareX*, 2022, **19**, 101101, DOI: **10.1016/j.softx.2022.101101**.

23 P. Xing, G. P. Robertson, M. D. Guiver, S. D. Mikhailenko, K. Wang and S. Kaliaguine, Synthesis and Characterization of Sulfonated Poly(Ether Ether Ketone) for Proton Exchange Membranes, *J. Membr. Sci.*, 2004, **229**(1–2), 95–106, DOI: **10.1016/j.memsci.2003.09.019**.

24 G. Wu, S.-J. Lin, I.-C. Hsu, J.-Y. Su and D. W. Chen, Study of High Performance Sulfonated Polyether Ether Ketone Composite Electrolyte Membranes, *Polymers*, 2019, **11**(7), 1177, DOI: **10.3390/polym11071177**.

25 E. M. Davis, J. Kim, V. P. Oleshko, K. A. Page and C. L. Soles, Uncovering the Structure of Nafion-SiO_2 Hybrid Ionomer Membranes for Prospective Large-Scale Energy Storage Devices, *Adv. Funct. Mater.*, 2015, **25**(26), 4064–4075, DOI: **10.1002/adfm.201501116**.

26 B. Schwenzer, J. Zhang, S. Kim, L. Li, J. Liu and Z. Yang, Membrane Development for Vanadium Redox Flow Batteries, *ChemSusChem*, 2011, **4**(10), 1388–1406, DOI: **10.1002/cssc.201100068**.

27 B. Schwenzer, S. Kim, M. Vijayakumar, Z. Yang and J. Liu, Correlation of Structural Differences between Nafion/Polyaniline and Nafion/Polypyrrole Composite Membranes and Observed Transport Properties, *J. Membr. Sci.*, 2011, **372**(1–2), 11–19, DOI: **10.1016/j.memsci.2011.01.025**.

28 G. M. Shashidhara and K. N. Kumar, Proton Conductivity of SPEEK Membranes, *Polym.-Plast. Technol. Eng.*, 2010, **49**(8), 796–806, DOI: **10.1080/03602551003749601**.

29 L. J. Anderson, X. Yuan, G. B. Fahs and R. B. Moore, Blocky Ionomers via Sulfonation of Poly(Ether Ether Ketone) in the Semicrystalline Gel State, *Macromolecules*, 2018, **51**(16), 6226–6237, DOI: **10.1021/acs.macromol.8b01152**.

30 B. Liu, W. Hu, G. P. Robertson and M. D. Guiver, Poly(Aryl Ether Ketone)s with Carboxylic Acid Groups: Synthesis, Sulfonation and Crosslinking, *J. Mater. Chem.*, 2008, **18**(39), 4675, DOI: **10.1039/b806690f**.

31 C. Wang, Z. Feng, Y. Zhao, X. Li, W. Li, X. Xie, S. Wang and H. Hou, Preparation and Properties of Ion Exchange Membranes for PEMFC with Sulfonic and Carboxylic Acid Groups Based on Polynorbornenes, *Int. J. Hydrogen Energy*, 2017, **42**(50), 29988–29994, DOI: **10.1016/j.ijhydene.2017.09.168**.

32 Z. Li, X. Liu, D. Chao, X. Lu, L. He, Y. Yang and W. Zhang, Crosslinked Sulfonated Poly(Arylene Ether Ketone) with Pendant Carboxylic Acid Group via Poly(Ethylene Glycol) for Proton Exchange Membrane, *J. Appl. Polym. Sci.*, 2010, **118**(6), 3318–3323, DOI: **10.1002/app.32439**.

33 J. Wang, S. Jiang, H. Zhang, W. Lv, X. Yang and Z. Jiang, Enhancing Proton Conduction and Methanol Barrier Performance of Sulfonated Poly(Ether Ether Ketone) Membrane by Incorporated Polymer Carboxylic Acid Spheres, *J. Membr. Sci.*, 2010, **364**(1–2), 253–262, DOI: **10.1016/j.memsci.2010.08.026**.

34 X. Wu, X. Wang, G. He and J. Benziger, Differences in Water Sorption and Proton Conductivity between Nafion and SPEEK, *J. Polym. Sci. B Polym. Phys.*, 2011, **49**(20), 1437–1445, DOI: **10.1002/polb.22326**.

35 J. Kamcev, D. R. Paul and B. D. Freeman, Effect of Fixed Charge Group Concentration on Equilibrium Ion Sorption in Ion Exchange Membranes, *J. Mater. Chem. A*, 2017, **5**(9), 4638–4650, DOI: **10.1039/C6TA07954G**.

36 F. G. Donnan, The Theory of Membrane Equilibria, *Chem. Rev.*, 1924, **1**(1), 73–90, DOI: **10.1021/cr60001a003**.

37 A. Domhoff, T. B. Martin, M. S. Silva, M. Saberi, S. Creager and E. M. Davis, Enhanced Proton Selectivity in Ionomer Nanocomposites Containing Hydrophobically Functionalized Silica Nanoparticles, *Macromolecules*, 2021, **54**(1), 440–449, DOI: **10.1021/acs.macromol.0c01696**.

38 W. Zhao, L.-P. Xiao, G. Song, R.-C. Sun, L. He, S. Singh, B. A. Simmons and G. Cheng, From Lignin Subunits to Aggregates: Insights into Lignin Solubilization, *Green Chem.*, 2017, **19**(14), 3272–3281, DOI: **10.1039/C7GC00944E**.

39 A. Duval, F. Vilaplana, C. Crestini and M. Lawoko, Solvent Screening for the Fractionation of Industrial Kraft Lignin, *Holzforschung*, 2016, **70**(1), 11–20, DOI: **10.1515/hf-2014-0346**.

40 G. P. Robertson, S. D. Mikhailenko, K. Wang, P. Xing, M. D. Guiver and S. Kaliaguine, Casting Solvent Interactions with Sulfonated Poly(Ether Ether Ketone) during Proton Exchange Membrane Fabrication, *J. Membr. Sci.*, 2003, **219**(1–2), 113–121, DOI: **10.1016/S0376-7388(03)00193-5**.

41 Md. M. Hossain and L. Aldous, Ionic Liquids for Lignin Processing: Dissolution, Isolation, and Conversion, *Aust. J. Chem.*, 2012, **65**(11), 1465, DOI: **10.1071/CH12324**.

42 S. Bylin, T. Wells, Q. Sun, A. Ragauskas and H. Theliander, Lignin Structure and Aggregation Behavior in a Two-

Component Ionic Liquid Solvent System, *BioResources*, 2014, **9**(4), 6002–6018, DOI: 10.15376/biores.9.4.6002-6018.

43 W. E. S. Hart, J. B. Harper and L. Aldous, The Effect of Changing the Components of an Ionic Liquid upon the Solubility of Lignin, *Green Chem.*, 2015, **17**(1), 214–218, DOI: 10.1039/C4GC01888E.

44 C. Jiang, H. He, X. Yao, P. Yu, L. Zhou and D. Jia, The Aggregation Structure Regulation of Lignin by Chemical Modification and Its Effect on the Property of Lignin/Styrene-Butadiene Rubber Composites, *J. Appl. Polym. Sci.*, 2018, **135**(5), 45759, DOI: 10.1002/app.45759.

45 M. Norgren, H. Edlund and L. Wågberg, Aggregation of Lignin Derivatives under Alkaline Conditions. Kinetics and Aggregate Structure, *Langmuir*, 2002, **18**(7), 2859–2865, DOI: 10.1021/la011627d.

46 S. Kubo and J. F. Kadla, Hydrogen Bonding in Lignin: A Fourier Transform Infrared Model Compound Study, *Biomacromolecules*, 2005, **6**, 2815–2821.

47 D. Tian, J. Hu, R. P. Chandra, J. N. Saddler and C. Lu, Valorizing Recalcitrant Cellulolytic Enzyme Lignin via Lignin Nanoparticles Fabrication in an Integrated Biorefinery, *ACS Sustainable Chem. Eng.*, 2017, **5**(3), 2702–2710, DOI: 10.1021/acssuschemeng.6b03043.

48 Y. Qian, Y. Deng, X. Qiu, H. Li and D. Yang, Formation of Uniform Colloidal Spheres from Lignin, a Renewable Resource Recovered from Pulping Spent Liquor, *Green Chem.*, 2014, **16**(4), 2156, DOI: 10.1039/c3gc42131g.

49 G. Gebel, Structure of Membranes for Fuel Cells: SANS and SAXS Analyses of Sulfonated PEEK Membranes and Solutions, *Macromolecules*, 2013, **46**(15), 6057–6066, DOI: 10.1021/ma400314c.

50 C. Zhao, H. Lin, K. Shao, X. Li, H. Ni, Z. Wang and H. Na, Block Sulfonated Poly(Ether Ether Ketone)s (SPEEK) Ionomers with High Ion-Exchange Capacities for Proton Exchange Membranes, *J. Power Sources*, 2006, **162**(2), 1003–1009, DOI: 10.1016/j.jpowsour.2006.07.055.

51 B. Yang and A. Manthiram, Comparison of the Small Angle X-Ray Scattering Study of Sulfonated Poly(Etheretherketone) and Nafion Membranes for Direct Methanol Fuel Cells, *J. Power Sources*, 2006, **153**(1), 29–35, DOI: 10.1016/j.jpowsour.2005.03.185.

52 G. Gebel, Structural Evolution of Water Swollen Perfluorosulfonated Ionomers from Dry Membrane to Solution, *Polymer*, 2000, **41**(15), 5829–5838, DOI: 10.1016/S0032-3861(99)00770-3.

53 K. Kreuer and G. Portale, A Critical Revision of the Nano-Morphology of Proton Conducting Ionomers and Polyelectrolytes for Fuel Cell Applications, *Adv. Funct. Mater.*, 2013, **23**(43), 5390–5397, DOI: 10.1002/adfm.201300376.

54 A. Kusoglu and A. Z. Weber, New Insights into Perfluorinated Sulfonic-Acid Ionomers, *Chem. Rev.*, 2017, **117**(3), 987–1104, DOI: 10.1021/acs.chemrev.6b00159.

55 Z. Zhu and S. J. Paddison, Perspective: Morphology and Ion Transport in Ion-Containing Polymers from Multiscale Modeling and Simulations, *Front. Chem.*, 2022, **10**, 981508, DOI: 10.3389/fchem.2022.981508.

56 G. Dorenbos, Doping Proton Transport Channels in Poly-Electrolyte Membranes with High Acidic Site Density Polymers, *Eur. Polym. J.*, 2017, **97**, 14–25, DOI: 10.1016/j.eurpolymj.2017.09.040.

57 O. Glatter, Modern Methods of Data Analysis in Small-Angle Scattering and Light Scattering, in *Modern Aspects of Small-Angle Scattering*, ed. H. Brumberger, Springer Netherlands, Dordrecht, 1995, pp 107–180, DOI: 10.1007/978-94-015-8457-9_4.

58 H. Mendil-Jakani, I. Zamanillo Lopez, P. M. Legrand, V. H. Mareau and L. Gonon, A New Interpretation of SAXS Peaks in Sulfonated Poly(Ether Ether Ketone) (sPEEK) Membranes for Fuel Cells, *Phys. Chem. Chem. Phys.*, 2014, **16**(23), 11243–11250, DOI: 10.1039/C4CP00710G.

59 M. Vijayakumar, S. D. Burton, C. Huang, L. Li, Z. Yang, G. L. Graff, J. Liu, J. Hu and M. Skyllas-Kazacos, Nuclear Magnetic Resonance Studies on Vanadium(IV) Electrolyte Solutions for Vanadium Redox Flow Battery, *J. Power Sources*, 2010, **195**(22), 7709–7717, DOI: 10.1016/j.jpowsour.2010.05.008.

60 K. Smith, F. Foglia, A. J. Clancy, D. J. L. Brett and T. S. Miller, Nafion Matrix and Ionic Domain Tuning for High-Performance Composite Proton Exchange Membranes, *Adv. Funct. Mater.*, 2023, **33**(42), 2304061, DOI: 10.1002/adfm.202304061.

61 G. Porod, O. Kratky, O. Glatter, *Small-Angle X-Ray Scattering*, London, Academic Press, 1982.

62 M. Yoonessi, H. Heinz, T. D. Dang and Z. Bai, Morphology of Sulfonated Polyarylenethioethersulfone Random Copolymer Series as Proton Exchange Fuel Cells Membranes by Small Angle Neutron Scattering, *Polymer*, 2011, **52**(24), 5615–5621, DOI: 10.1016/j.polymer.2011.09.047.

63 G. Gebel and J. Lambard, Small-Angle Scattering Study of Water-Swollen Perfluorinated Ionomer Membranes, *Macromolecules*, 1997, **30**(25), 7914–7920, DOI: 10.1021/ma970801v.

64 A.-L. Rollet, O. Diat and G. Gebel, A New Insight into Nafion Structure, *J. Phys. Chem. B*, 2002, **106**(12), 3033–3036, DOI: 10.1021/jp020245t.

65 M. M. Schiavone, O. Tarallo, R. Di Girolamo, L. Caporaso, M.-S. Appavou, Z. Revay and A. Radulescu, Structure and Morphology of Model Polymer Electrolyte Membranes Based on Sulfonated Syndiotactic-Polystyrene in the δ Co-Crystalline Phase Resolved by Small-Angle Neutron Scattering, *Solid State Ionics*, 2018, **320**, 392–406, DOI: 10.1016/j.ssi.2018.03.022.

66 S. Yun, J. Parrondo, F. Zhang and V. Ramani, Microstructure-Property Relationships in Sulfonated Polyether Ether Ketone/Silsesquioxane Composite Membranes for Direct Methanol Fuel Cells, *J. Electrochem. Soc.*, 2014, **161**(9), F815–F822, DOI: 10.1149/2.0021409jes.

67 G. Beaucage, Small-Angle Scattering from Polymeric Mass Fractals of Arbitrary Mass-Fractal Dimension, *J. Appl. Crystallogr.*, 1996, **29**(2), 134–146, DOI: 10.1107/S0021889895011605.